# Dark Matter and Dark Energy from a single scalar field and CMB data.

Roberto Mainini, Loris P.L. Colombo & Silvio A. Bonometto

*Physics Department G. Occhialini, Università degli Studi di Milano–Bicocca, Piazza della Scienza 3, I20126 Milano (Italy) & I.N.F.N., Sezione di Milano*



## ABSTRACT

Axions are likely to be the Dark Matter (DM) that cosmological data require. They arise in the Peccei–Quinn solution of the strong–$CP$ problem. In a previous work we showed that their model has a simple and natural generalization which yields also Dark Energy (DE), in fair proportions, without tuning any parameter: DM and DE arise from a single scalar field and are weakly coupled in the present era. In this paper we extend the analysis of this *dual–axion* cosmology and fit it to WMAP data, by using a Markov chain technique. We find that ΛCDM, dynamical DE with a SUGRA potential, DE with a SUGRA potential and a constant DE–DM coupling, *as well as the dual–axion model* with a SUGRA potential, fit data with a similar accuracy. The best–fit parameters are however fairly different, although consistency is mostly recovered at the 2–$\sigma$ level. A peculiarity of the dual–axion model with SUGRA potential is to cause more stringent constraints on most parameters and to favor high values of the Hubble parameter.

*Subject headings:* cosmology: theory – dark energy

## 1. Introduction

Models with density parameters $\Omega_{o,de} \simeq 0.7$, $\Omega_{o,m} \simeq 0.3$, $\Omega_{o,b} \simeq 0.04$ (for dark energy, whole non–relativistic matter and baryons, respectively), Hubble parameter $h \simeq 0.7$ (in units of 100 km/s/Mpc) and primeval spectral index $n_s \simeq 1$ fit most cosmological data, including Cosmic Microwave Background (CMB) anisotropies, large scale structure, as well as data on SNIa (Tegmark et al. 2001, De Bernardis et al. 2000, Hanany et al. 2000, Halverson et al. 2001, Spergel et al. 2003, Percival et al. 2002, Efstathiou et al. 2002, Riess et al. 1988, Perlmutter et al. 1988). The success of such ΛCDM models, also dubbed cosmic concordance models, does not hide their uneasiness. The parameters of standard CDM are still to be increased by one, in order to tune Dark Energy (DE). Furthermore, if DE is ascribed to vacuum, this turns out to be quite a fine tuning.

This conceptual problem was eased by dynamical DE models (Wetterich 1988, 1995; Ratra & Peebles 1988, RP hereafter). They postulate the existence of an *ad–hoc* scalar field, self–interacting through a suitable effective potential, which depends on a further parameter. In RP and SUGRA (see below) models, this is an energy scale $\Lambda$ (or an exponent $\alpha$).

Within the frame of dynamical DE models, Mainini & Bonometto (2004, MB hereafter) tried to take a step forward. Instead of invoking an *ad–hoc* interaction, they refer to the field introduced by Peccei & Quinn (1977, PQ hereafter) to solve the strong–CP problem. If suitably tuned, such scheme was already shown to yield DM (Preskill, Wise & Wilczek 1983, Abbott & Sikivie 1983, Dine & Fischler 1983). MB slightly modify the PQ scheme, replacing the Nambu–Goldstone (NG) potential introduced *ad–hoc*, by a potential admitting a tracker solution. This scheme solves the strong–CP problem even more efficiently than the original PQ model. The $\Lambda$ parameter of the tracker potential takes the place of the PQ energy scale, $F_{PQ}$. Fixing it in the range solving the strong–CP problem yields DM and DE in fair proportions. Here, we shall call this cosmology *dual–axion* model. This model has several advantages both in respect to $\Lambda$CDM and ordinary dynamical DE: (i) it requires no fine tuning; (ii) it adds no parameter to the standard PQ scheme, which yields just DM; (iii) it introduces no field or interaction, besides those required by particle physics. This scheme, however, leads to predictions (slightly) different from $\Lambda$CDM, for a number of observables. In principle, therefore, it can be falsified by data.

The essential peculiarity of the model is that it predicts a coupling between DM and DE. Coupled DE models were introduced by a number of authors (see, e.g., Amendola 2000, 2003; Gasperini, Piazza & Veneziano 2002; Perrotta & Baccigalupi 2002) as no direct evidence exists that DM particles follow geodesics. Most such models, however, introduce a further coupling parameter $\beta$. Its tuning fixes DM–DE coupling within an acceptable range. For instance, Amendola & Quercellini (2003) give limits on $\beta$ deduced from a fit to WMAP data (Spergel et al 2003); Macciò et al. (2004) restricted $\beta$ even more, by studying the halo profiles, produced in N–body simulations with coupled DE.

At variance from these pictures, the dual–axion scheme has no extra coupling parameter. The strength of the coupling is set by theory and, if this conflicts with data, the whole scheme is falsified. The only degree of freedom still allowed is the choice of the tracker potential. This freedom exists for any dynamical DE model. Also PQ exploited it by choosing a NG potential. For the sake of definiteness, up to now, the dual–axion scheme has been explored just in association with a SUGRA potential. MB showed that, in this case, the dual axion scheme predicts a fair growth of density fluctuations, so granting a viable picture for the Large Scale Structure.

The recent detailed WMAP data on CMB anisotropies allow to submit the dual–axion model to further stringent tests, by comparing it with other cosmologies as $\Lambda$CDM, standard and interacting dynamical DE. This is done here by using a multiparameter Markov chain technique (see, e.g., Kosowski et al. 2003; Christensen et al. 2001; Knox et al. 2002; Lewis et al. 2002). The results of this numerical approach will then be discussed and understood on physical bases. None of the above models however performs neatly better than the others. Apparently, the best fit is obtained by dynamical DE based on a SUGRA potential, but its success is strictly marginal. The analysis of these models against CMB data is the main aim of this paper.

The plan of the paper is as follows: In Section 2 we summarize the particle physics background

to the dual axion model. In particular, starting from Section 2.3, we restrict our analysis to a particular form of DE potential, the SUGRA potential; using a different potential might change some quantitative results. In Section 3 we describe the technique used to compare different models with CMB data and present (subsection 3.2) the results of this comparison. Section 4 is devoted to a final discussion of the results.

## 2. A single scalar field to account for DM and DE

Let us first remind that the strong $CP$ problem arises from the existence in QCD (quantum–chromo–dynamics) of multiple vacuum states. The set of the gauge transformations $\Omega(x_i)$ that join vacuum configurations can be subdivided in classes $\Omega_n(x_i)$, characterized by an integer $n$ (Jackiw & Rebbi 1976), setting their different asymptotic behaviors. Within each class, transformations can be distorted into each other with continuity, while this is impossible if they pertain to different classes.

Accordingly, in classical field theory there is no communication between different–$n$ gauge sectors. In quantum field theory, instead, tunneling is possible thanks to instanton effects, so that any vacuum state is a superposition of the vacua $|0_n\rangle$ (of the $n$th sector), of the kind $|0_\theta\rangle = \sum_n |0_n\rangle \exp(in\theta)$.

The effects of varying the $\theta$–vacuum can be recast into variations of a non–perturbative term

$$\mathcal{L}_\theta = \frac{\alpha_s}{2\pi}\theta\, G\cdot\tilde{G} \tag{1}$$

($\alpha_s$: strong coupling constant, $G$ and $\tilde{G}$: gluon field tensor and its dual) in the QCD Lagrangian density. However, chiral transformations also change the vacuum angle, so that the $\theta$–parameter receives another contribution, arising from the EW (electro-weak) sector, when the quark mass matrix $\mathcal{M}$ is diagonalized, becoming

$$\theta_{eff} = \theta + Arg\ det\ \mathcal{M}\ . \tag{2}$$

The Lagrangian term (1) can be reset in the form of a 4–divergence and causes no change of the equations of motion. It however violates $CP$ and, among various effects, yields a neutron electric moment $d_n \simeq 5\cdot 10^{-16}\theta_{eff}$ e cm, conflicting with the experimental limit $d_n \lesssim 10^{-25}$ e cm, unless $\theta_{eff} \lesssim 10^{-10}$.

The point is that the two contributions to $\theta_{eff}$ are uncorrelated, so that there is no reason why their sum should be so small.

PQ succeed in suppressing this term by imposing an additional global chiral symmetry $U(1)_{PQ}$, spontaneously broken at a suitable scale $F_{PQ}$. The axion field is suitably coupled to the quark sector. The details of this coupling depend on the model and may require the introduction of an *ad–hoc* heavy quark (Kim 1979, Shifman et al. 1979, see also Dine et al. 1981, Zhitnisky 1980).

The $U(1)_{PQ}$ symmetry suffers from a chiral anomaly, so the axion acquires a tiny mass because of non-perturbative effects, whose size has a rapid increase around the quark-hadron transition scale $\Lambda_{QCD}$. The anomaly manifests itself when a chiral $U(1)_{PQ}$ transformation is performed on the axion field, giving rise to a term of the same form of (1), which provides a potential for the axion field.

As a result, $\theta$ is effectively replaced by the dynamical axion field. Its oscillations about the potential minimum yield axions. This mechanism works independently of the scale $F_{PQ}$. Limits on it arise from astrophysics and cosmology, requiring that $10^{10}GeV \lesssim F_{PQ} \lesssim 10^{12}GeV$; in turn, this yields an axion mass which lays today in the interval $10^{-6}eV \lesssim m_A \lesssim 10^{-3}eV$.

More in detail, in most axion models, the PQ symmetry breaking occurs when a complex scalar field $\Phi = \phi e^{i\theta}/\sqrt{2}$, falling into one of the degenerated minima of a NG potential

$$V(\Phi) = \lambda[|\phi|^2 - F_{PQ}^2]^2 \ , \tag{3}$$

develops a vacuum expectation value $\langle\phi\rangle = F_{PQ}$.

The $CP$-violating term, arising around quark-hadron transition when $\bar{q}q$ condensates break the chiral symmetry, reads

$$V_1 = \left[\sum_q \langle 0(T)|\bar{q}q|0(T)\rangle m_q\right] \ (1 - \cos\theta) \tag{4}$$

($\sum_q$ extends over all quarks), so that $\theta$ is no longer arbitrary, but shall be ruled by a suitable equation of motion. The term in square brackets, at $T \simeq 0$, approaches $m_\pi^2 f_\pi^2$ ($m_\pi$ and $f_\pi$: $\pi$–meson mass and decay constant). In this limit, for $\theta \ll 1$ and using $A = \theta F_{PQ}$ as axion field, eq. (4) reads:

$$V_1 \simeq \frac{1}{2} q^2(m_q) m_\pi^2 f_\pi^2 \frac{A^2}{F_{PQ}^2} \ ; \tag{5}$$

here $q(m_q)$ is a function of the quark masses $q_i$; in the limit of 2 light quarks ($u$ and $d$), $q = \sqrt{m_u/m_d}(1 + m_u/m_d)^{-1}$. The $A$ field bears the right dimensions but, here below, will no longer be used, and the axion degrees of freedom will be described through $\theta$ itself. Eq. (5), however, shows that, when $\langle\bar{q}q\rangle$ is no longer zero (since $T \lesssim \Lambda_{QCD}$), the axion mass decreases with temperature approaching the constant value $m_A = m_\pi f_\pi q(m_q)/F_{PQ}$ for $T \ll \Lambda_{QCD}$.

Accordingly, the equation of motion, in the small $\theta$ limit, reads

$$\ddot{\theta} + 2\frac{\dot{a}}{a}\dot{\theta} + a^2 m_A^2 \theta = 0 \ , \tag{6}$$

(here $a$ is the scale factor and dots yield differentiation with respect to conformal time, see next Section), so that the axion field undergoes (nearly) harmonic oscillations, as soon as $m_A$ exceeds

the expansion rate; then, his mean pressure vanishes (Dine & Fischler 1983) leaving axion as a viable candidate for cold DM.

MB replace the NG potential in eq. (3) by a potential $V(\Phi)$ admitting a tracker solution (Wetterich 1988,1995, RP 1988, Ferreira & Joyce 1998, Brax & Martin 1999, 2001, Brax, Martin & Riazuelo 2000). The field $\Phi$ is complex and $V(\Phi)$ is $U(1)$ invariant, but there is no transition to a constant value $F_{PQ}$, which is replaced by the modulus $\phi$ itself, slowly evolving over cosmological times. At a suitable early time, quantum dynamics starts to be fairly accounted by the potential $V$; soon after, $\phi$ settles on the tracker solution in almost any horizon, however breaking the $U(1)$ symmetry, by the values assumed by $\theta$, in different horizons. Later on, when chiral symmetry breaks, dynamics becomes relevant also for the $\theta$ degree of freedom, as in the PQ case. At variance from it, however, this happens while $\phi$ continues its slow evolution, down to the present epoch, when it accounts for DE. Owing to the $\phi$ evolution, however, the axion mass evolves, over cosmological times, also for $T \ll \Lambda_{QCD}$ (see below).

The $\Phi$ field, therefore, besides of providing DM through its phase $\theta$, whose dynamics solves the strong $CP$ problem, also accounts for DE through its modulus $\phi$.

This scheme holds for any DE potential admitting tracker solutions. To be more specific, MB use a SUGRA potential (Brax, Martin & Riazuelo 2000; Brax & Martin 1999; Brax & Martin 2001) finding that, at the quark–hadron transition, $\phi$ can be naturally led to have values $\sim F_{PQ}$, increasing up to $\sim m_p = G^{-1/2}$ (the Planck mass), when approaching today. The only free parameter is the energy scale in the SUGRA potential, that must be $\sim 10^{10}$GeV. With this choice, $\theta$ is driven to values even smaller than in the PQ case, so that $CP$ is apparently conserved in strong interactions, while $\Omega_{o,m}$, $\Omega_{o,de}$ (the DE density parameter) and $\Omega_{o,b}$ take fair values.

### 2.1. Lagrangian theory

In the dual–axion model we start from the Lagrangian

$$\mathcal{L} = \sqrt{-g}\{g_{\mu\nu}\partial_\mu\Phi\partial_\nu\Phi - V(\phi)\} \ , \tag{7}$$

which can be rewritten in terms of $\phi$ and $\theta$, adding also the term breaking the $U(1)$ symmetry. Then it reads:

$$\mathcal{L} = \sqrt{-g}\left\{\frac{1}{2}g_{\mu\nu}[\partial_\mu\phi\partial_\nu\phi + \phi^2\partial_\mu\theta\partial_\nu\theta] - V(\phi) - m^2(T,\phi)\phi^2(1-\cos\theta)\right\} \ . \tag{8}$$

Here $g_{\mu\nu}$ is the metric tensor. We shall assume that $ds^2 = g_{\mu\nu}dx^\mu dx^\nu = a^2(d\tau^2 - \eta_{ij}dx_i dx_j)$, so that $a$ is the scale factor, $\tau$ is the conformal time; Greek (Latin) indexes run from 0 to 3 (1 to 3); dots indicate differentiation in respect to $\tau$. The mass behavior for $T \sim \Lambda_{QCD}$ will be detailed in Section 2.2. The equations of motion, for the $\phi$ and $\theta$ degrees of freedom, read

$$\ddot{\theta} + 2\left(\frac{\dot{a}}{a} + \frac{\dot{\phi}}{\phi}\right)\dot{\theta} + m^2a^2\sin\theta = 0 \ , \tag{9}$$

$$\ddot{\phi} + 2\frac{\dot{a}}{a}\dot{\phi} + a^2 V'(\phi) = \phi\,\dot{\theta}^2 \ . \tag{10}$$

(Notice that $m^2(T,\phi)\phi^2$ is $\phi$ independent, see below.) In what follows, the former equation will be always considered when $\sin\theta \simeq \theta$. In particular, taking into account the condition $\theta \ll 1$, the expressions for the energy densities $\rho_{\theta,\phi} = \rho_{\theta,\phi;kin} + \rho_{\theta,\phi;pot}$ and the pressures $p_{\theta,\phi} = \rho_{\theta,\phi;kin} - \rho_{\theta,\phi;pot}$ are obtainable by combining the terms

$$\rho_{\theta,kin} = \frac{\phi^2}{2a^2}\dot{\theta}^2 \ , \quad \rho_{\theta,pot} = m^2(T,\phi)\phi^2(1-\cos\theta) \simeq \frac{m^2(T,\phi)}{2}\phi^2\theta^2 \ ,$$
$$\rho_{\phi,kin} = \frac{\dot{\phi}^2}{2a^2} \quad , \qquad \rho_{\phi,pot} = V(\phi) \ . \tag{11}$$

When $\theta$ undergoes many (nearly) harmonic oscillations within a Hubble time, $\langle\rho_{\theta,kin}\rangle \simeq \langle\rho_{\theta,pot}\rangle$ and $\langle p_\theta\rangle$ vanishes (Dine & Fischler 1983). Under such condition, using eqs. (9) and (10), it is easy to see that

$$\dot{\rho}_\theta + 3\frac{\dot{a}}{a}\rho_\theta = \frac{\dot{m}}{m}\rho_\theta \ , \quad \dot{\rho}_\phi + 3\frac{\dot{a}}{a}(\rho_\phi + p_\phi) = -\frac{\dot{m}}{m}\rho_\theta \ . \tag{12}$$

When $m$ is given by eq. (15) and (16) here below, $\dot{m}/m = -\dot{\phi}/\phi - 3.8\,\dot{T}/T$. At $T \simeq 0$, instead, it is just $\dot{m}/m \simeq -\dot{\phi}/\phi$.

The $\theta$ and $\phi$ components account for DM and DE, respectively. Accordingly, in the sequel, the indexes $_\theta$, $_\phi$ will be replaced by $_{dm}$, $_{de}$.

Eqs. (12) clearly show that an exchange of energy occurs between DM and DE. From this point of view, the MB model belongs to the set of coupled models treated by Amendola (2000, 2003). It is however characterized by a time–dependent coupling. In fact, in the small $\theta$ limit, after averaging over cosmological times, the r.h.s. of eqs. (10) and (12) read $C(\phi)\langle\rho_\theta\rangle a^2$ and $\pm C(\phi)\,\dot{\phi}\,\langle\rho_\theta\rangle$, if we set $C(\phi) = 1/\phi$. Here $C$ is the DE–DM coupling introduced by Amendola (2000, 2003), who however studies extensively only the case $C = \beta(16\pi/3m_p^2)^{1/2}$, with constant $\beta$. In these latter DE models, a $\phi$–$MDE$ phase takes place after matter–radiation equivalence. It differs from a matter dominated expansion because of the contribution of the kinetic part of the DE field to the expansion source. A regime of this kind is present also in the dual–axion model and is shown in Fig. 5, here below. Because of the $\phi$ dependence, however, the DM–DE coupling, in the dual–axion model, weakens as we approach the present cosmological epoch.

The most stringent limits on $\beta$ are set by non–linear predictions (Macciò et al. 2004) and restrict $\beta$ to values $\lesssim$ 0.1–0.2 , in order to avoid a too high concentration in DM halos. In turn, this is due to the behavior of the effective mass of DM particles, in the presence of the $\beta$–coupling. A preliminary inspection indicates that the behavior expected here is opposite and that halo concentrations, in average, should be smaller than in ΛCDM. This point, however, must be inspected in much more detail.

Let us also notice that the former eq. (12) can be integrated soon, yielding $\rho_{dm} \propto m/a^3$. In particular, this law holds at $T \ll \Lambda_{QCD}$. Accordingly, at late times

$$\rho_{dm} a^3 \phi \simeq \text{const.}, \tag{13}$$

so that the usual behavior $\rho_{dm} \propto a^{-3}$ is modified by the energy outflow from DM to DE. This modification is stronger when $\phi$ varies rapidly and is damped when $\phi$ attains a nearly constant behavior.

### 2.2. Axion mass

According to eq. (9), the axion field begins to oscillate when:

$$m(T,\phi)a \simeq 2\left(\frac{\dot{a}}{a}+\frac{\dot{\phi}}{\phi}\right) \ . \tag{14}$$

In the dual–axion model, just as for PQ, the axion mass rapidly increases when the chiral symmetry is broken by the formation of the $\bar{q}q$ condensate at $T \sim \Lambda_{QCD}$. In the dual–axion model, however, the axion mass varies also later on, because of the evolution of $\phi$, when $m(T,\phi)$ is

$$m_o(\phi) = \frac{q(m_q)\, m_\pi f_\pi}{\phi} \simeq \frac{\mu_{QCD}^2}{\phi} \ ; \tag{15}$$

with $\mu_{QCD} \simeq 80\,\mathrm{MeV}$. Since $\phi \sim m_p$ today, the present axion mass $m_a \sim 5 \cdot 10^{-13}$eV. At high temperature, according to Gross et al. (1981),

$$m(T,\phi) \simeq 0.1\, m_o(\phi) \left(\frac{\Lambda_{QCD}}{T}\right)^{3.8} \tag{16}$$

This expression must be interpolated with eq. (15), to study the fluctuation onset for $T \sim \Lambda_{QCD}$. We report the results of the solution of the equations in Sec. 2.1, obtained by assuming

$$m(T,\phi) = \ m_o(\phi) \left(\frac{0.1^{\,1/3.8}\,\Lambda_{QCD}}{T}\right)^{3.8(1-a/a_c)} \qquad a < a_c \tag{17}$$

$$m(T,\phi) = m_o(\phi) \qquad a > a_c \tag{18}$$

with $a_c = T_o/\Lambda_{QCD}\, 0.1^{1/3.8} = 2.16 \cdot 10^{-12}$; here $T_o = 2.35 \cdot 10^{-4}\,\mathrm{eV}$, $\Lambda_{QCD} = 200\,\mathrm{MeV} \simeq 2.5\,\mu_{QCD}$. The expressions (17), (18) assure that $m(T,\phi)$ and its first derivative are continuous and that the axion mass meets its low–$T$ behavior $m_o(T)$ at $T \simeq 0.55\,\Lambda_{QCD}$. The effects of selecting a different value for $\Lambda_{QCD}$ were studied. Also the impact of the assumed $T$ dependence was considered. A change of $\Lambda_{QCD}$, by a factor 2, yields a variation of $\Lambda$ in the SUGRA potential (see next section) by not more than a few percent. Taking a power $\nu \neq 1$ of $(1 - a/a_c)$, in the exponent, instead, does not affect continuity but changes the rapidity by which the high–$T$ regime (16) is met. In Fig. 4 we plot both the interpolated mass behavior and the first $\theta$ oscillations. Changing $\nu$ just slightly displaces the interpolating curve between $\sim a_{QCD}$ and $\sim 1.5\, a_{QCD}$, causing a minor phase shift. Let us finally outline that eqs. (15) and (16), as well as the interpolation (17),(18), assure that $m(T,\phi)\phi$ is $\phi$–independent, as is required to give the equation of motion the form (10).

### 2.3. Using the SUGRA potential

Most above features are general and do not depend on the choice of the potential $V$. We shall now assume that

$$V(\Phi) = \frac{\Lambda^{\alpha+4}}{\phi^\alpha} \exp\left(\frac{4\pi\phi^2}{m_p^2}\right) \tag{19}$$

(SUGRA potential; see Brax & Martin 1999, 2001, Brax, Martin & Riazuelo 2000). Apparently $V(\Phi)$ depends on the two parameters $\Lambda$ and $\alpha$. When they are independently assigned, $\Omega_{de}$ is also fixed. Here we prefer to use $\Omega_{de}$ and $\Lambda$ as independent parameters. The latter scale is related to $\alpha$ as shown in Figure 1. This relation is almost independent from the presence of DE–DM coupling. The slight shifts due to the couplings, evaluated through the expressions of this paper, are just slightly above the numerical noise and are also shown in Figure 1.

The potential (19) does not depend on $\theta$ and, in the radiation dominated era, admits the tracker solution

$$\phi^{\alpha+2} = g_\alpha \Lambda^{\alpha+4} a^2 \tau^2 \ , \tag{20}$$

with $g_\alpha = \alpha(\alpha+2)^2/4(\alpha+6)$. This tracker solution, characterizing SUGRA models at very high $z$, is abandoned, because of the DE–DM coupling, when the term $\phi\dot{\theta}^2$ exceeds $a^2V'$, and the field enters a different tracking regime:

$$\phi^2 = \frac{1}{2}\rho_{dm} a^2 \tau^2 \ . \tag{21}$$

Fig. 2 is a landscape behavior of densities, starting from the high–$z$ tracking regime (20), passing then to the new intermediate tracking regime, and reaching the regimes when DE density eventually exceeds first radiation ($z \sim 100$), then baryons (at $z \sim 10$) and DM (at $z \sim 3$). In Fig. 3, we show the evolution of the DE–field $\phi$. In Fig. 4, we focus on the Q–H transition and magnify the scale dependence of the mass and the onset of $\theta$ oscillations. Finally, in Fig. 5, we show the behaviors of the density parameters $\Omega_i$ ($i = r,\ b,\ \theta,\ \phi$, *i.e.* radiation, baryons, DM, DE) *vs.* the scale factor $a$. More detailed pictures of the single transitions are shown in MB.

### 2.4. Parameter fixing

In general, once $\Omega_{o,de}$ and $h$ are given, a model with dynamical (coupled or uncoupled) DE is not yet determined, as $\alpha$ or $\Lambda$ are still to be fixed. When fitting WMAP data, here below, we shall mostly refer to the energy scale $\Lambda$ and remind that, when $\Omega_{o,de}$ and $\Lambda$ are given also $\alpha$ is fixed.

Other potentials show similar features and this implies that, in general, dynamical DE models depend on one more parameter than, e.g., ΛCDM; accordingly, one can expect that they more easily accommodate observational data. In principle, data fitting is even more facilitated by DM–DE coupling, which adds a further parameter (the strength of coupling) to the theoretical plot.

In the dual–axion model with a SUGRA potential, no such arbitrariness exists. If this model, where a suitable DM–DE coupling is present, succeeds in fitting observational data, this will not be

favored by extra parameters. The coupling, in particular, depends on no parameter and the very scale $\Lambda$ is set by theoretical consistency arguments, similarly to what happens for the $F_{PQ}$ scale in the PQ approach.

Let us follow the behavior of $\rho_{dm}$, backwards in time, until the very beginning of the oscillatory regime, when the approximation $\theta \ll 1$ begins to hold. Using the scaling law (13) until then and, at earlier times, the more general laws (11), together with eq. (14), we build a system yielding the scale factor $a_h$ when the fluctuations start, and the scale $\Lambda$ in the SUGRA potential (19).

It turns out that $a_h$ and $\Lambda$ are almost independent from $\Omega_{o,dm}$ and $h$, and we shall now outline the qualitative reasons of this feature. According to eqs. (11) and (15), at the $a_h$ scale it must be

$$\rho_{h,dm} \simeq m_h^2\, \phi^2(a_h)\; \epsilon^2(a_h) = \left(\frac{m_h}{m_o}\right)^2 \mu_{QCD}^4\, \epsilon^2(a_h)\;, \tag{22}$$

where $m_h = m(a_h)$, while $\epsilon^2 \equiv 2\langle(1-\cos\theta)\rangle$ is $\sim \theta^2$ when the oscillatory regime is onset. Owing to eq. (14), however, the oscillation onset occurs when the axion mass is approximately the inverse of $a_h\tau(a_h)$ and the latter quantity can be related to the temperature $T_h$, via the Friedmann equation. This yields that $T_h^2 \simeq m_p m_h/8$ and, using again eq. (15), that

$$T_h \simeq 5\cdot 10^{-2}\mu_{QCD}\left(\frac{m_p}{\phi_h}\frac{m_h}{m_o}\right)^{1/2}\;. \tag{23}$$

Let us now assume that it is now $\phi \sim m_p$ and use the law (13) from now to $a_h$. It is then

$$T_h \simeq \mu_{QCD}\left[\frac{5\cdot 10^3}{\Omega_{o,dm}h^2}\left(\frac{m_h}{m_o}\right)^3 \epsilon^2(a_h)\right]^{\frac{1}{5}}\;, \tag{24}$$

provided that $\mu_{QCD} \simeq 4\cdot 10^{11} T_o$ and $\rho_{o,dm} \simeq 3\cdot 10^4 T_o^4 \Omega_{o,dm} h^2$.

The temperature $T_h$ (and the scale $a_h$) are then essentially model independent because of the power 1/5 at the l.h.s. of eq. (24). If we consider the plots in Fig. 4, obtained through a numerical integration for $\Omega_{o,dm} = 0.27$ and $h = 0.7$, we see that $(m_h/m_o)^3\epsilon^2 \sim 10^{-2}$–$10^{-3}$, so that $T_h$ falls around $\Lambda_{QCD}$. However, no appreciable displacement can be expected just varying $\Omega_{o,dm}$ and $h$, even though we suppose that this induces substantial variations of the factor $(m_h/m_o)^3\,\epsilon^2(a_h)$ which, however, cannot exceed unity or lay below $\sim 10^{-3}$.

The model independence of $a_h$ implies that the scale $\Lambda$ is also almost model independent. The numerical result $a_h \simeq 10^{-13}$ is consistent with $\Lambda \simeq 1.5\cdot 10^{10}$GeV, but neither value will change much just by varying $\Omega_{o,dm}$. In practice, when $\Omega_{o,dm}$ goes from 0.2 to 0.4, $\log_{10}(\Lambda/\mathrm{GeV})$ (almost) linearly runs from 10.05 to 10.39 and $a_h$ steadily lays at the eve of the quark–hadron transition.

The residual dependence of $\alpha$ and $\Lambda$ on $\Omega_{o,dm}$ is plotted in Fig. 6, together with the corresponding values for $w$ at $z = 0$. Significantly smaller values for $\Lambda$ are obtainable only for unphysically small DM densities.

The only way to modify the result is to consider values of $\phi$ significantly different from $m_p$, today. In fact, the rest of the plot can be understood as an effect of the position reached by the $\phi$ field, in the SUGRA potential, at the present time. The peak of $w$ corresponds to a maximum of kinetic energy and occurs if the minimum of SUGRA potential is attained today. Today lays in the proximity of the minimum for a fairly wide $\Lambda$ interval. Accordingly, a significant $\Lambda$ variation, thereabout, yields just a modest shift of $\Omega_{o,dm}$, as is shown in the lower plot. For still greater $\Lambda$'s, $\phi$ would still be in its pre–minimum descent. For even smaller amounts of DE, the present $\phi$ configuration would still lay in the $\phi$-MD era, when kinetic energy dominates for DE, although the very DE contribution to the overall energy density becomes negligible.

A model with DE and DM given by a single complex field, based on a SUGRA potential, therefore bears a precise prediction on the scale $\Lambda$, for the observational $\Omega_{o,dm}$ range. Moreover, just the observational $\Omega_{o,dm}$ range (0.2–0.4) corresponds to $\phi \sim m_p$ today.

The rest of this paper is devoted to a comparison of this and other models against WMAP data. In such comparison, however, the scale $\Lambda$ shall not be fixed, *a priori*, in the expected range. In general, the dual axion model belongs to a wider class of coupled DM–DE models, which can be dubbed $\phi^{-1}$–models because of the shape of the coupling, where the scale $\Lambda$ is left free.

The features of $\phi^{-1}$ models, in general, are quite reasonable. They have two independent dark components, DM and DE, suitably coupled, about whose nature no assumption is made, just as in standard coupled DE models. In the latter models, however, the strength of the coupling is gauged by an extra parameter $\beta$. $\phi^{-1}$ models, from this point of view, already offer less freedom, as $C \equiv \phi^{-1}$ and no coupling modulation is allowed.

Should the comparison of $\phi^{-1}$ models with WMAP data favor parameter values compatible with cosmological observables and values of $\Lambda$ compatible with the dual–axion model, this means that WMAP data support the origin of DE and DM that the dual–axion model suggests.

## 3. Comparison with WMAP data

WMAP data have been extensively used to provide tight constraints on cosmological parameters. They consists of high precision estimates of the anisotropy power spectrum $C_l^T$ up to $l \sim 900$, as well of the TE correlation power spectrum $C_l^{TE}$ up to $l \sim 450$. We shall use these data to constrain possible cosmologies, in a parameter space of 7 to 8 dimensions. A grid-based likelihood analysis would then require prohibitive amounts of CPU time and we use a Markov Chain Monte Carlo (MCMC) approach, as it has become customary for CMB analysis (e.g., Christensen et al. 2001; Knox et al. 2002; Lewis et al. 2002; Kosowski et al. 2002; Dunkley et al. 2004).

The principal analysis of WMAP first–year data (Spergel et al. 2003) constrained flat $\Lambda$CDM models defined by six parameters: $\Omega_{o,b}h^2$, $\Omega_{o,m}h^2$, $h$, $n$, the fluctuation amplitude $A$ and the optical depth $\tau$. Notice that, with the naming convention used here, $\Omega_{o,m} \equiv \Omega_{o,b} + \Omega_{o,dm}$. As possible

extensions of ΛCDM cosmologies, several works considered models with a fixed state parameter $w \equiv p_{de}/\rho_{de}$ (e.g., Spergel et al. 2003; Bean & Dorè 2004; Tegmark et al. 2004; Melchiorri 2004), or adopted $z$–dependent parameterizations of $w(z)$ interpolating between early–time and late–time values (e.g., Corasaniti et al. 2004; Jassal et al. 2004; Rapetti et al. 2004). A general conclusion was that current data mostly allow to constrain only the present state parameter, $w(z=0) \lesssim -0.80$.

In this work we consider, instead, three classes of dynamical DE, requiring the introduction of additional parameters specifying the physical properties of the scalar field. (i) SUGRA dynamical DE require the introduction of $\lambda = \log_{10}(\Lambda/\mathrm{GeV})$, yielding the energy scale in the potential (12). (ii) In constant coupling DE, the coupling parameter $\beta = C\,(3m_p^2/16\pi)^{1/2}$ is also needed. (iii) In the case of the dual–axion model, the last parameter is excluded, for it is simply $C = \phi^{-1}$. Also the scale $\Lambda$ is constrained by the requirement that $\Omega_{o,de}$ lays in a fair range (also solving the strong $CP$ problem). Hence, in the dual–axion model, $\Lambda$ and $\Omega_{o,de}$ are no longer independent parameters. We however consider a wider class of coupled DE models, that we call $\phi^{-1}$ models, leaving $\lambda$ as a free parameter. Our aim is to test whether WMAP data constrain it into the region turning a $\phi^{-1}$ model into a dual–axion model.

In the use of MCMC, as well as in any attempt to fit CMB data to models, a linear code providing $C_l$'s is needed. Here we use our optimized extension of CMBFAST (Seljak & Zaldarriaga 1996), able to inspect the cosmologies (i), (ii) and (iii). Then, the likelihood of each model is evaluated through the publicly available code by the WMAP team (Verde et al. 2003) and accompanying data (Hinshaw et al. 2003; Kogut et al. 2003).

### 3.1. Implementing a MCMC algorithm

A MCMC algorithm samples a known distribution $\mathcal{L}(\mathbf{x})$ by means of an arbitrary trial distribution $p(\mathbf{x})$. Here $\mathcal{L}$ is a likelihood and $\mathbf{x}$ is a point in the parameter space. The chain is started from a random position $\mathbf{x}$ and moves to a new position $\mathbf{x}'$, according to the trial distribution. The probability of accepting the new point is given by $\mathcal{L}(\mathbf{x}')/\mathcal{L}(\mathbf{x})$; if the new point is accepted, it is added to the chain and used as the starting position for a new step. If $\mathbf{x}'$ is rejected, a replica of $\mathbf{x}$ is added to the chain and a new $\mathbf{x}'$ is tested.

In the limit of infinitely long chains, the distribution of points sampled by a MCMC describes the underlying statistical process. Real chains, however, are finite and convergence criteria are critical. Moreover, a chain must be required to fully explore the high probability region in the parameter space. Statistical properties estimated using a chain which has yet to achieve good convergence or mixing may be misleading. Several methods exist to diagnose mixing and convergence, involving either single long chains or multiple chains starting from well separated points in the parameter space, as the one used here. Once a chain passes convergence tests, it is an accurate representation of the underlying distribution.

In order to ensure mixing, we run six chains of $\sim 30000$ points each, for each model cate-

gory. We diagnose convergence by requiring that, for each parameter, the variances both of the single chains and of the whole set of chains ($W$ and $B$, respectively) satisfy the Gelman & Rubin test (Verde et al. 2003; Gelman & Rubin 1992), $R < 1.1$ with:

$$R = \frac{[(N-1)/N]W + (1+1/M)B}{W} \ . \tag{25}$$

Here each chain has $2N$ points, but only the last $N$ points are used to estimate variances, and $M$ is the total number of chains. In most model categories considered, we find that the slowest parameter to converge is $\lambda$.

### 3.2. Results

The results of this paper mostly concern the fit of the double–axion model with WMAP data. Let us however also briefly outline the features of the model.

Quite in general, cosmological models fitting observations require a a triple coincidence between DM, baryon and DE densities, the last one occurring just at the present epoch. Any such coincidence requires the tuning of a suitable parameter. It is then natural to look for an underlying physics, able to predict the parameter values that cosmology requires.

If DM is made of axions, we must tune the $F_{PQ}$ parameter in the NG potential involving a $\Phi$ field, whose phase $\theta$ is then the axion field. Here we saw that the PQ model does not strictly require a NG potential. A potential causing no immediate settling at an energy minimum, but inducing a slow rolling along a tracking solution, achieves the same aims. If such potential is SUGRA, it contains an energy scale $\Lambda$ to be tuned, in stead of $F_{PQ}$. If this is done, so to yield the required amount of DM, this scheme provides, as an extra bonus, a fair amount of DE, which is prescribed to interact with DM in a peculiar way, never studied in the literature.

The possible shapes of DE–DM interaction considered up to now involved an *ad–hoc* coupling parameter. No such parameter exists here. For instance, a standard model of coupled SUGRA involves a density parameter $\Omega_{o,dm}$, an energy scale $\Lambda$ and a coupling parameter $\beta$. Here, not only $\beta$ no longer exists, but also $\Lambda$ is fixed once $\Omega_{0,dm}$ is assigned. The model is therefore highly constrained and data can easily falsify it. The only available degree of freedom, to modify it, amounts to replacing the SUGRA potential with another potential shape. Another reserve to be born in mind is that axion models have a contribution to DM coming from the decay of topological structures, which were not considered here.

These arguments outline the significance of the fit of the model with WMAP data. The basic results of this work concern this fit and are summarized in the Tables 1–3. For each model category we list the expectation values of each parameter and the associated variance; we also list the values of the parameters of the best fitting models. The corresponding marginalized distributions are plotted in figures 7–9, while joint 2D confidence regions are shown in figures 10–12.

The values of $\chi^2$, for each category of models can be compared, taking into account the number of degrees of freedom. This comparison is shown in Table 4. The smallest $\chi^2$ is obtained for the uncoupled SUGRA model, which performs slightly better than ΛCDM. Differences however are really small and yield no support to any model category.

It must be however reminded that the $\phi^{-1}$ models, whose fitting results are reported in Table 3 and Figures 9 and 12, include the dual–axion model, but many other cases as well. Our approach was meant to test whether CMB data carry information on $\lambda$ and how this information fits the $\lambda$ range turning a $\phi^{-1}$ model into the dual–axion model.

Let us also outline that Tables 1 and 2 and the corresponding figures, *concerning uncoupled or constant–coupling* SUGRA models, outline that WMAP data provide no real constraint on $\lambda = \log(\Lambda/\mathrm{GeV})$, when allowed to vary from $\sim -12$ to 16. No limitation exists even on its sign. On the contrary, when a $\phi^{-1}$ coupling is set, loose but precise limitations on $\lambda$ arise, as is shown in Table 3. In the presence of this coupling, the 2–$\sigma$ Λ–interval ranges from $\sim 10$ to $\sim 3 \cdot 10^{10}$GeV, *including the range required by the dual–axion model.*

In fact, in this case, the location of peaks in spectra is more strictly related to the $\phi$ evolution. In turn, only a restricted sect of Λ values allows an $l$–dependence of multipoles consistent with data. Fig. 13 shows this fact for anisotropy, while Figs. 14 and 15 are predictions for the TE and E–polarization spectra.

Fig. 13 also shows why no model category neatly prevails. At large $l$ all best–fit models yield similar behaviors. In turn this shows that discrimination could be achieved by improving large angular scale observation, especially for polarization, so to reduce errors on small–$l$ harmonics.

## 4. Discussion

Our analysis does not concern the double axion model only, but the whole spectrum of models built using a SUGRA potential. This is useful also to evaluate the significance of the fit of the dual–axion model.

### 4.1. Uncoupled and coupled SUGRA models

A first point we must therefore outline is that SUGRA *uncoupled* models are consistent with WMAP data. The ratio $w = p/\rho$, for most these models is $\lesssim -0.80$ at $z = 0$. However, they exhibit a fast variation of $w$, which already attains values $\sim -0.6$ at $z \sim 1$–2. This sharp decrease does not conflict with data and these models perform even better than ΛCDM. For uncoupled or constant–coupling SUGRA models, the analysis in the presence of priors leads to analogous conclusions.

Table 1: SUGRA parameters in the absence of DE–DM coupling: for each parameter $x$, the expectation value $\langle x \rangle$, variance $\sigma_x$, and maximum likelihood values $x_{max}$, in the 7–dimensional parameter space, are shown.

| $x$ | $\langle x \rangle$ | $\sigma_x$ | $x_{max}$ |
|---|---|---|---|
| $\Omega_{o,b}h^2$ | 0.025 | 0.001 | 0.026 |
| $\Omega_{o,dm}h^2$ | 0.12 | 0.02 | 0.11 |
| $h$ | 0.63 | 0.06 | 0.58 |
| $\tau$ | 0.21 | 0.07 | 0.28 |
| $n_s$ | 1.04 | 0.04 | 1.08 |
| $A$ | 0.97 | 0.13 | 1.11 |
| $\lambda$ | 3.0 | 7.7 | 13.7 |

Table 2: SUGRA parameters in the presence of a constant DE–DM coupling $\beta$: The parameter space is 7–dimensional and parameter values are shown as in the previous Table.

| $x$ | $\langle x \rangle$ | $\sigma_x$ | $x_{max}$ |
|---|---|---|---|
| $\Omega_{o,b}h^2$ | 0.024 | 0.001 | 0.024 |
| $\Omega_{o,dm}h^2$ | 0.11 | 0.02 | 0.12 |
| $h$ | 0.74 | 0.11 | 0.57 |
| $\tau$ | 0.18 | 0.07 | 0.17 |
| $n_s$ | 1.03 | 0.04 | 1.02 |
| $A$ | 0.92 | 0.14 | 0.93 |
| $\lambda$ | -0.5 | 7.6 | 8.3 |
| $\beta$ | 0.10 | 0.07 | 0.07 |

Table 3: SUGRA parameters for a $\phi^{-1}$ model. The parameter $\lambda$ is left arbitrary; at variance from other model categories, $\lambda$ here is constrained and consistency with the dual–axion model is recovered at $2\,\sigma$'s. Parameter values are shown as in Table 1.

| $x$ | $\langle x \rangle$ | $\sigma_x$ | $x_{max}$ |
|---|---|---|---|
| $\Omega_{o,b}h^2$ | 0.025 | 0.001 | 0.026 |
| $\Omega_{o,dm}h^2$ | 0.11 | 0.02 | 0.09 |
| $h$ | 0.93 | 0.05 | 0.98 |
| $\tau$ | 0.26 | 0.04 | 0.29 |
| $n_s$ | 1.23 | 0.04 | 1.23 |
| $A$ | 1.17 | 0.10 | 1.20 |
| $\lambda$ | 4.8 | 2.4 | 5.7 |

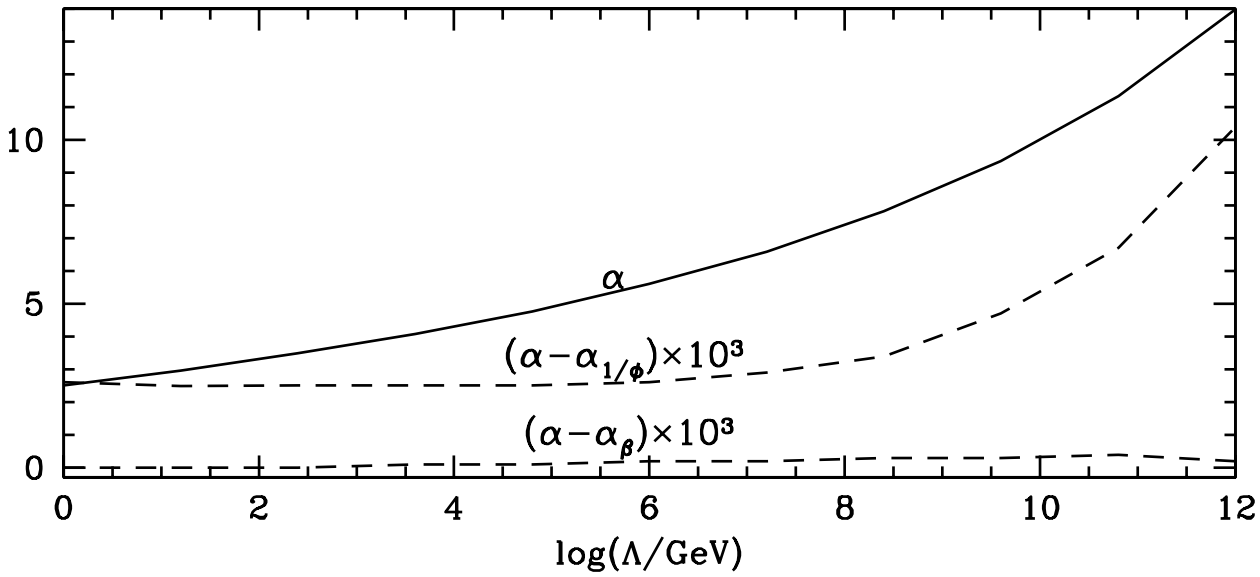


Fig. 1.— Values of $\alpha$ corresponding to given $\Lambda$ scales in SUGRA models with $\Omega_{o,dm} = 0.27$. The tiny differences, just above noise level, for coupled models ($\alpha_\beta$ and $\alpha_{1/\phi}$ for constant coupling and $\phi^{-1}$ coupling, respectively), are also shown.

Table 4: Goodness of fit. For each class of DE considered, Table lists the number of degrees of freedom (d.o.f.), the reduced $\chi^2_{eff}$, and the corresponding probability of the best–fit model. Figures for ΛCDM and dual–axion models are also included. ΛCDM models have 1342 degrees of freedom, uncoupled and $\phi^{-1}$ have 1341, while fixed–$\beta$ has 1340.

| | $\chi^2_{eff}$ | prob. |
|---|---|---|
| no coupling | 1.064 | 5.0 % |
| $\beta$–coupling | 1.066 | 4.7 % |
| $\phi^{-1}$–coupling | 1.074 | 2.9 % |
| dual–axion | 1.081 | 2.0 % |
| ΛCDM | 1.066 | 4.7 % |

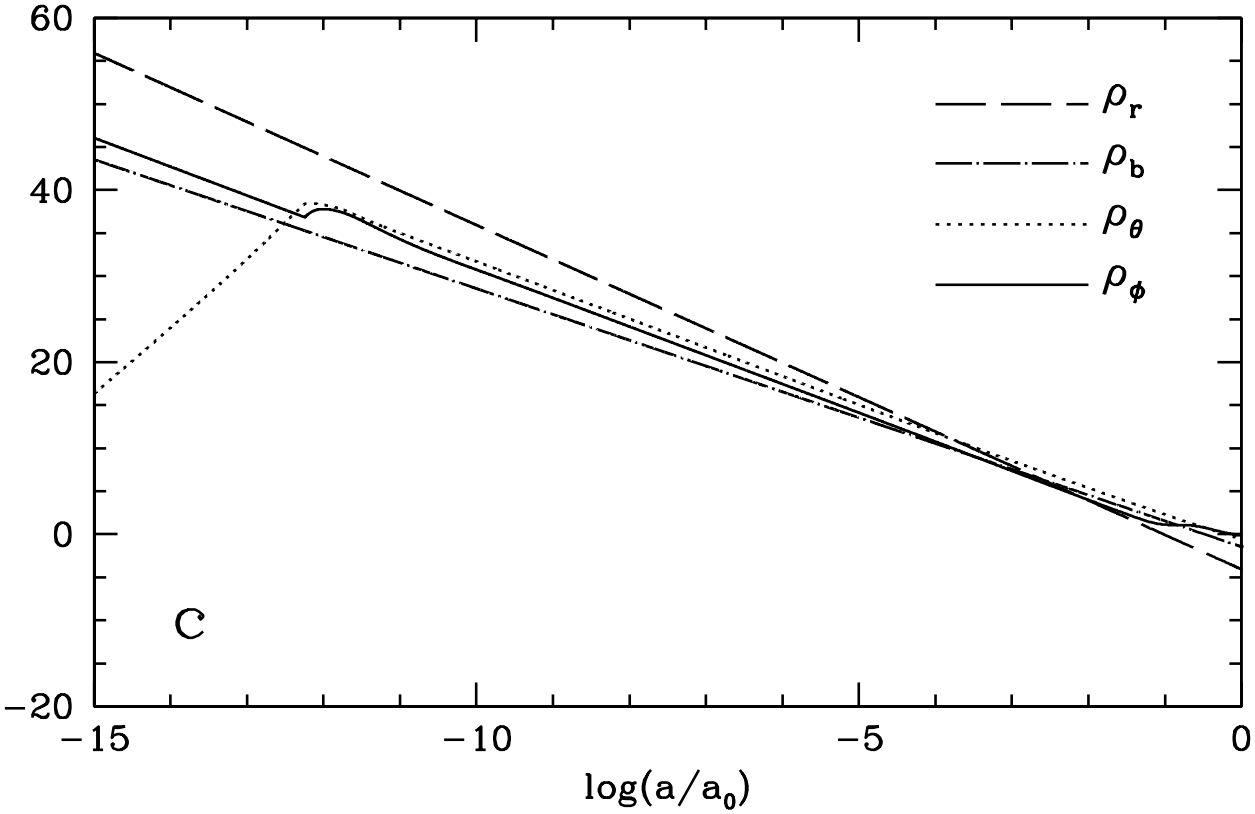


Fig. 2.— Behaviors of densities from the tracking regimes down to the regimes when DE density exceeds radiation ($z \sim 100$), baryons (at $z \sim 10$) and DM (at $z \sim 3$).

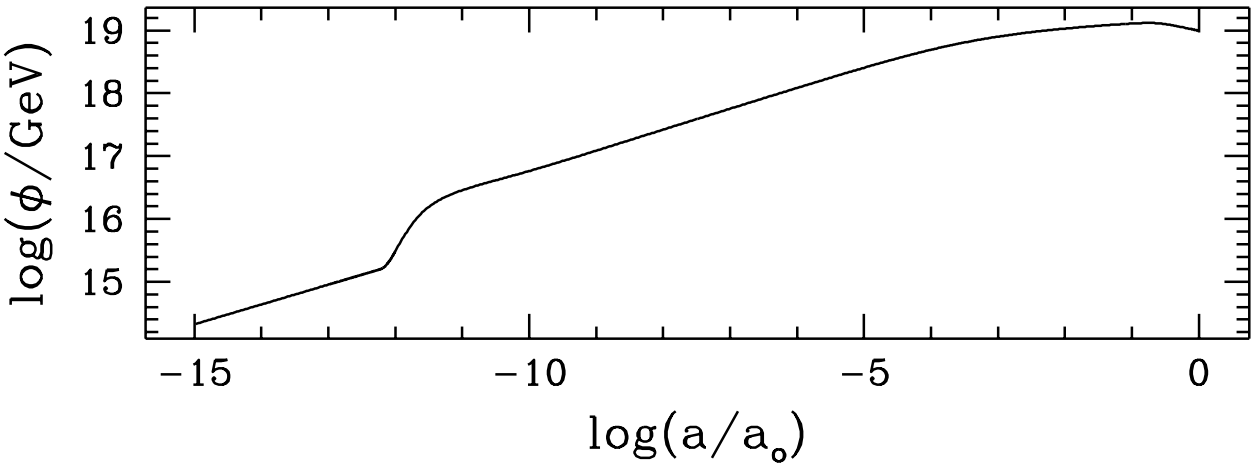


Fig. 3.— Evolution of the DE–field. Notice the jump around the QH scale and the low–$z$ rebounce.

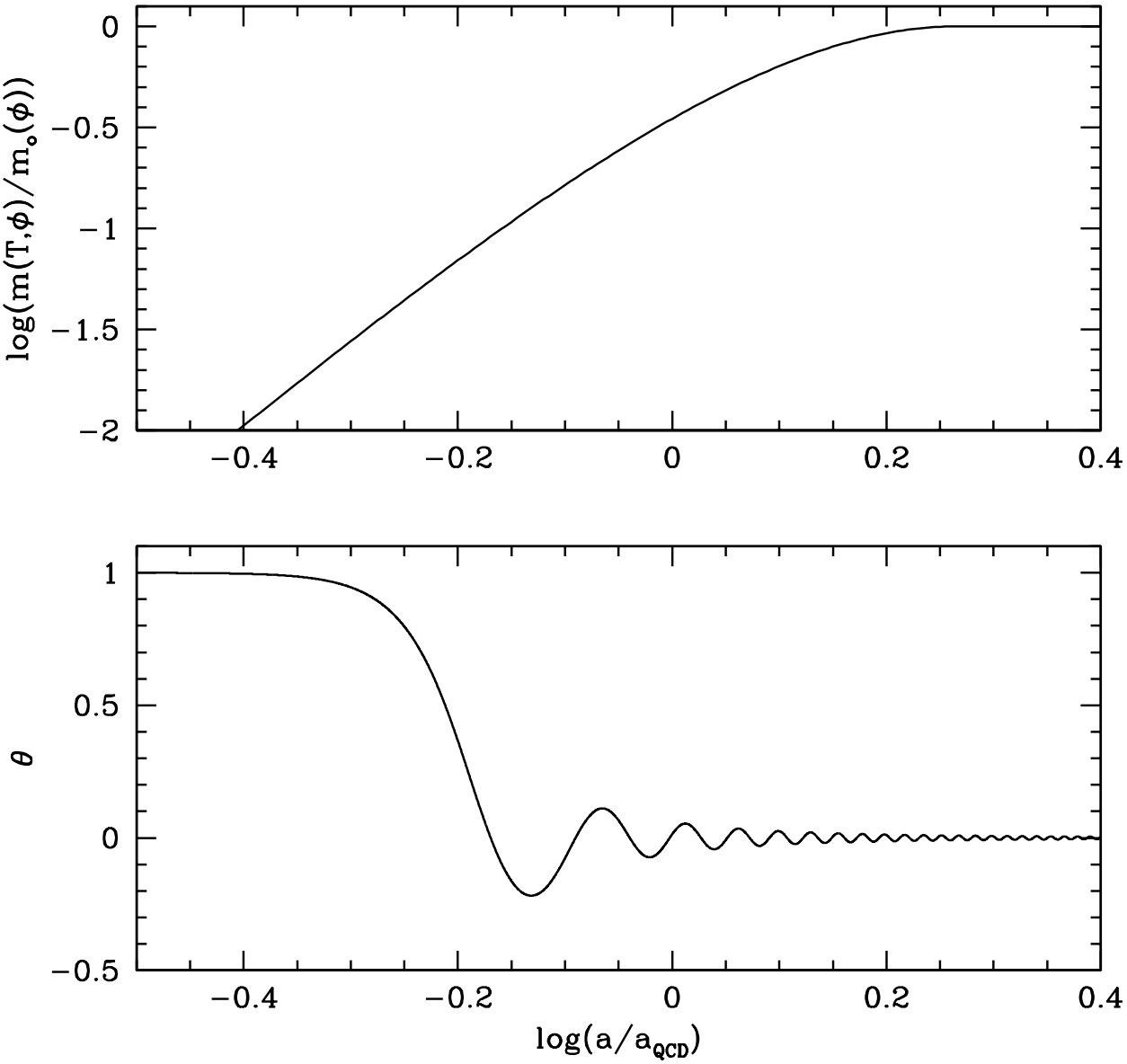


Fig. 4.— Interpolated mass behavior and first $\theta$ oscillations. $a_{QCD}$ is the scale when $T = \Lambda_{QCD}$.

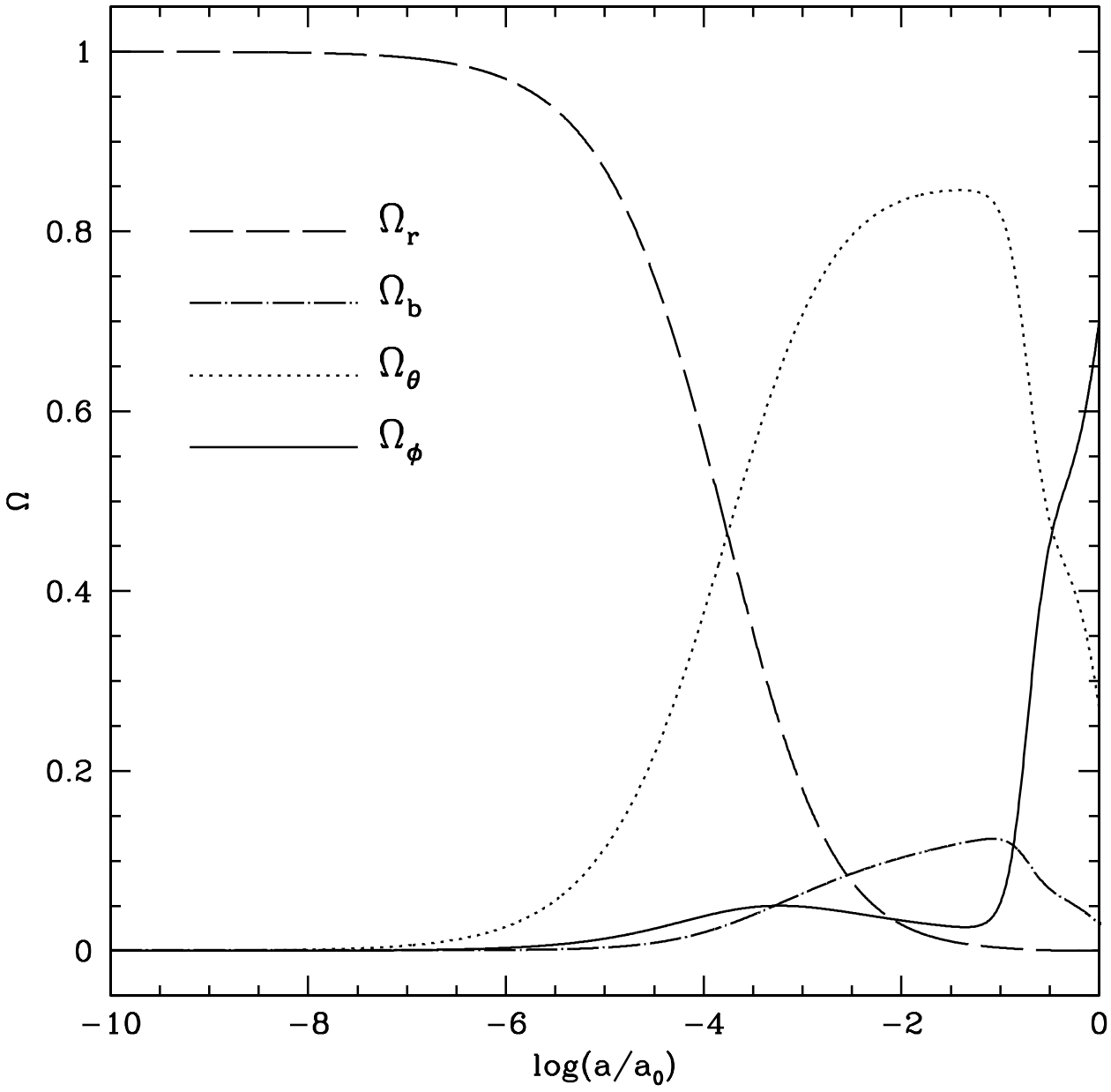


Fig. 5.— Density parameters $\Omega_i$ ($i = r,\ b,\ \theta,\ \phi$, *i.e.* radiation, baryons, DM, DE).

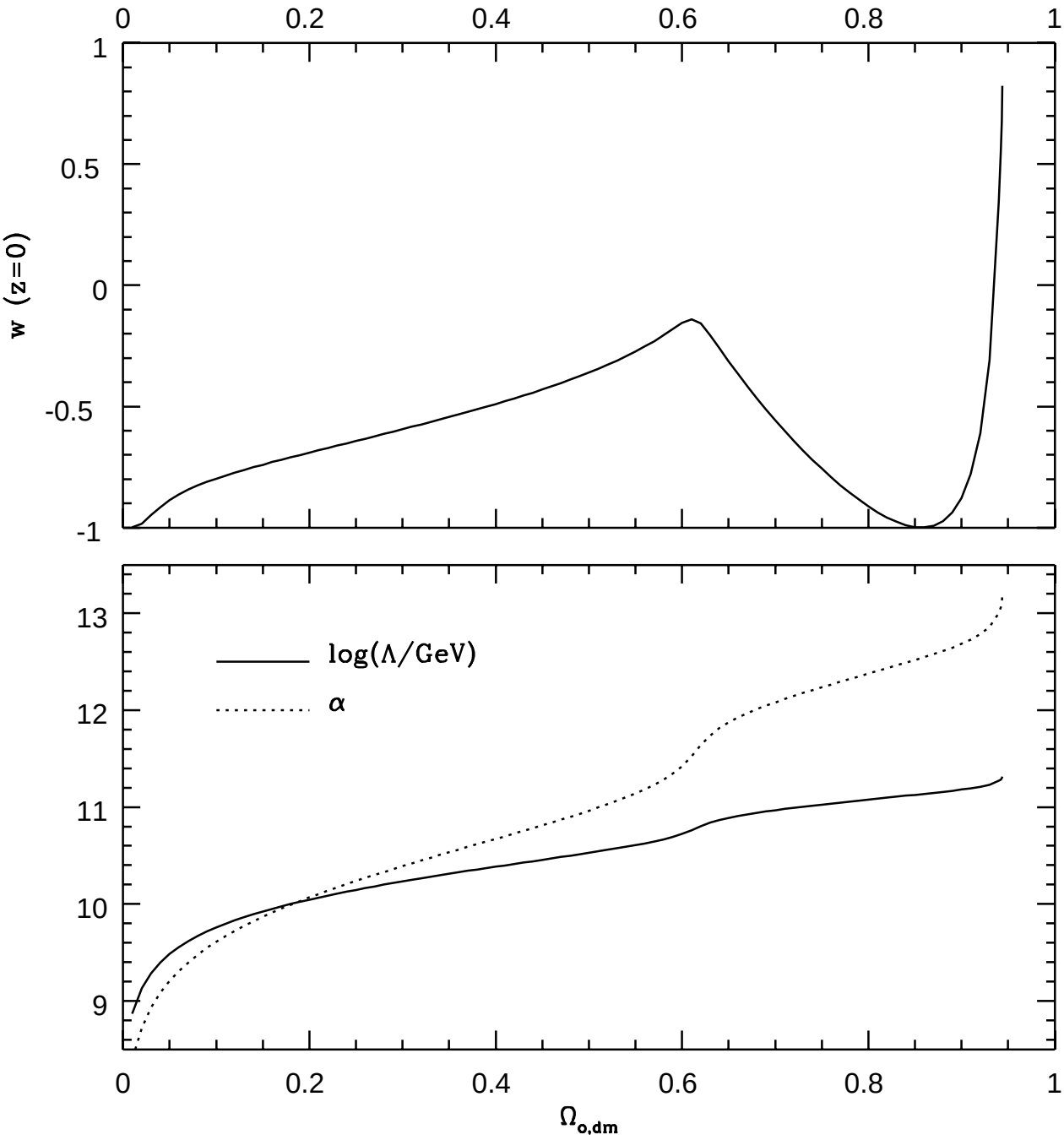


Fig. 6.— The lower plot shows the variation of the exponent $\alpha$ and the $\Lambda$ scale in the SUGRA potential, when varying the present fraction of DM. The faster $\Lambda$ increase, at $\Omega_{o,dm} \simeq 0.6$, is due to a stationary behavior in the set of models where the $\phi$ fields attains (approximately) today the minimum of the SUGRA potential. In fact, if it were $\Omega_{o,dm} \simeq 0.6$ today, the upper plot shows that $w$ would corresponds to top kinetic energy and minimum potential energy. These plots are obtained for $h = 0.7$.

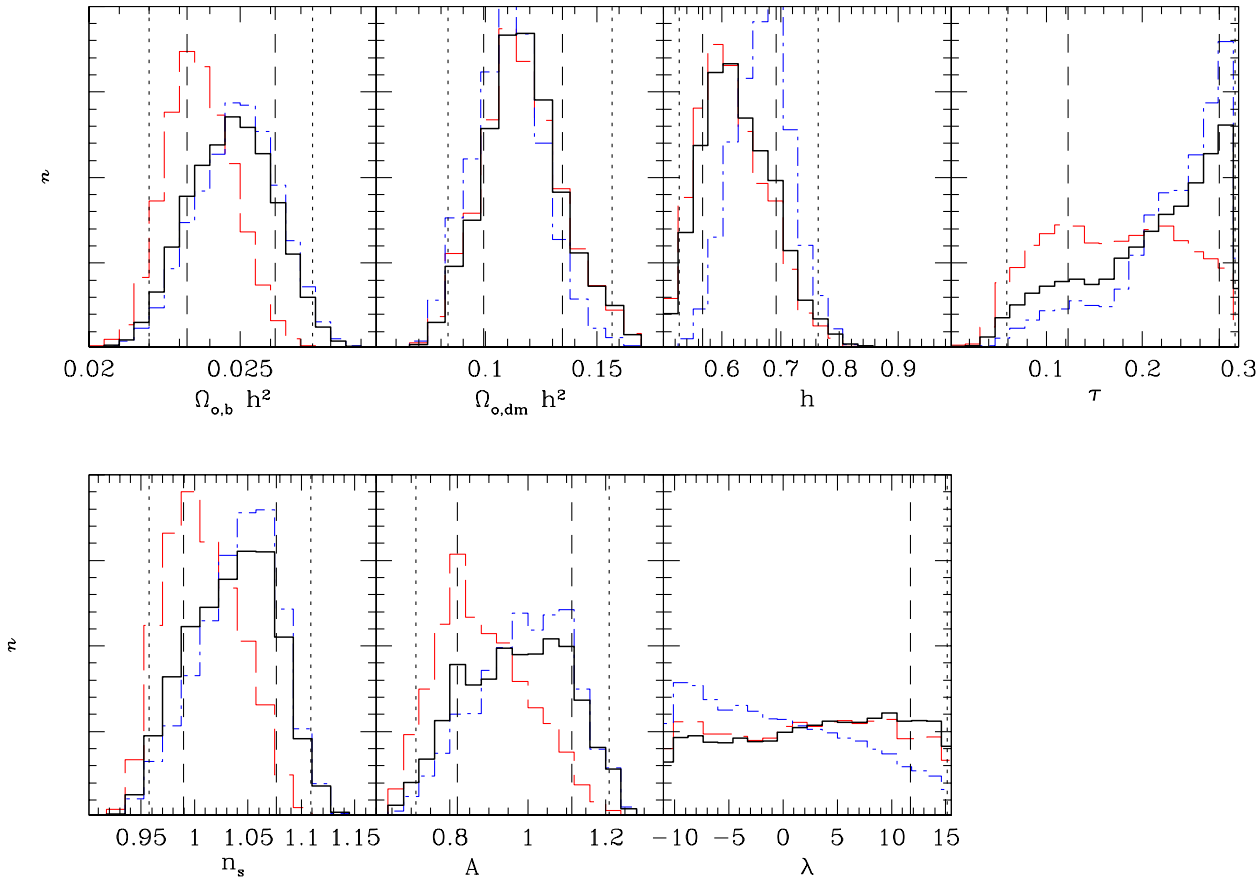


Fig. 7.— Marginalized distributions for the 7–parameters SUGRA model with no priors (solid lines), BBNS prior (long dashed) or HST prior (dot–dashed). Short dashed (dotted) vertical lines show the boundaries of 68.3 % c.l. (95.4 % c.l.) interval; for $\lambda$ only upper limits are shown.

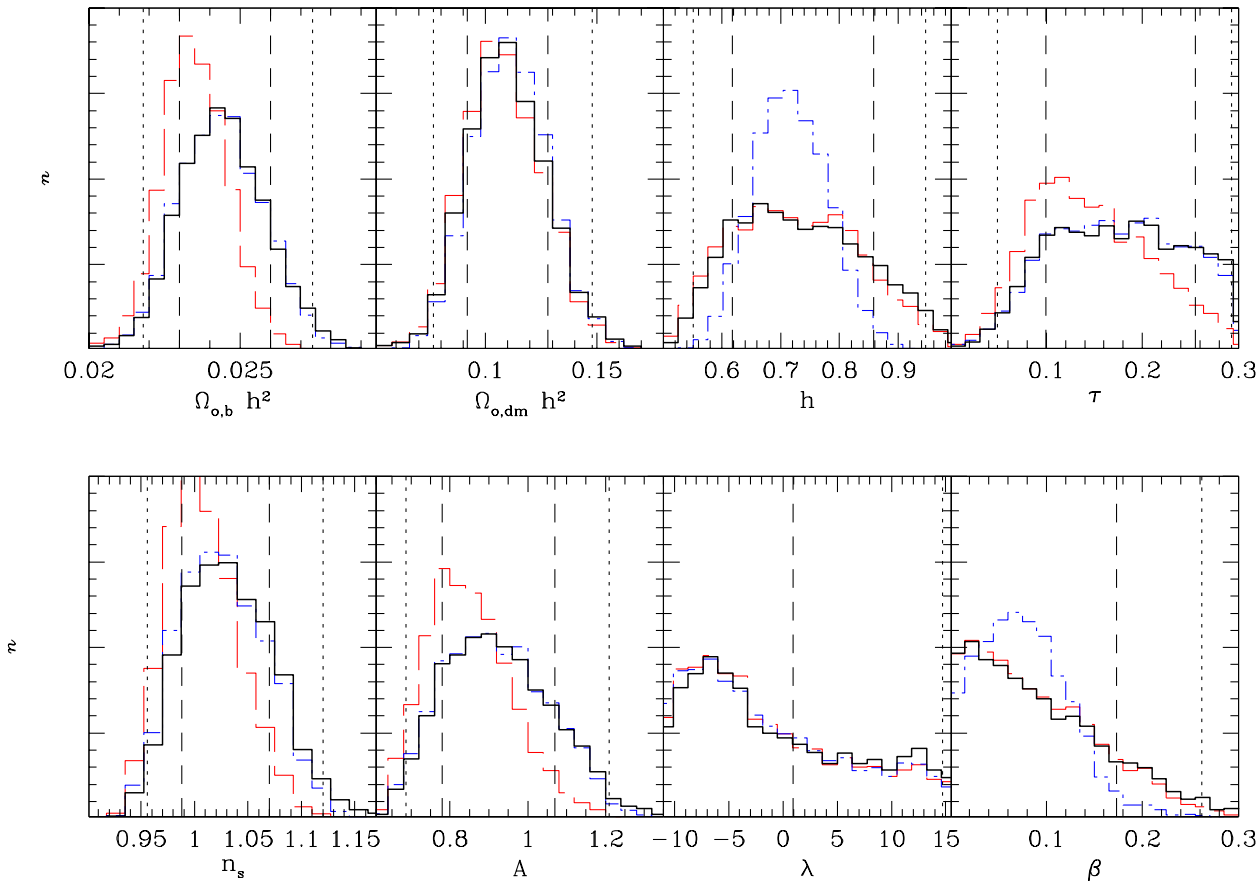


Fig. 8.— As Fig. 7 but for the 8–parameters constant coupling model. For $\lambda$ and $\beta$ only the upper c.l. boundaries are shown.

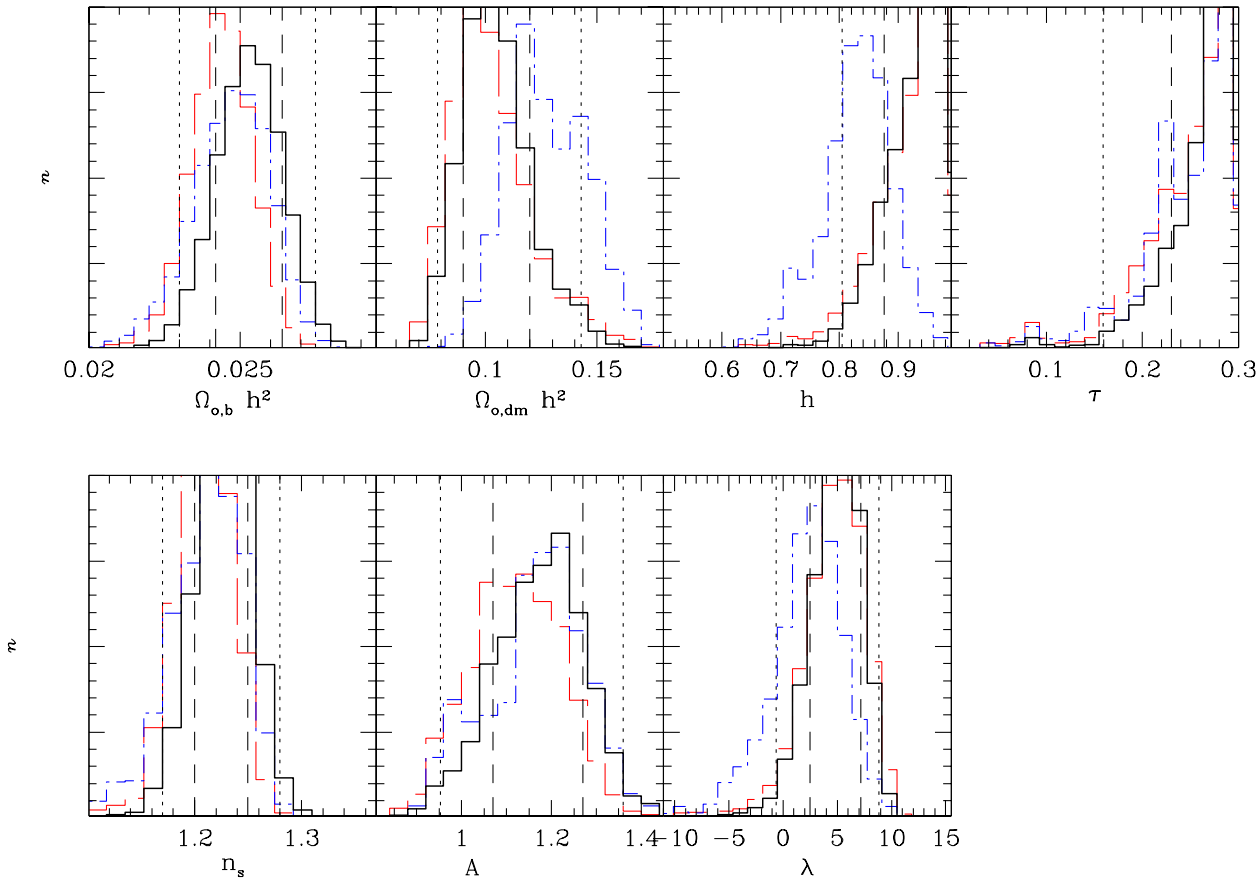


Fig. 9.— As Fig. 7 but for the 7–parameters $\phi^{-1}$ model.

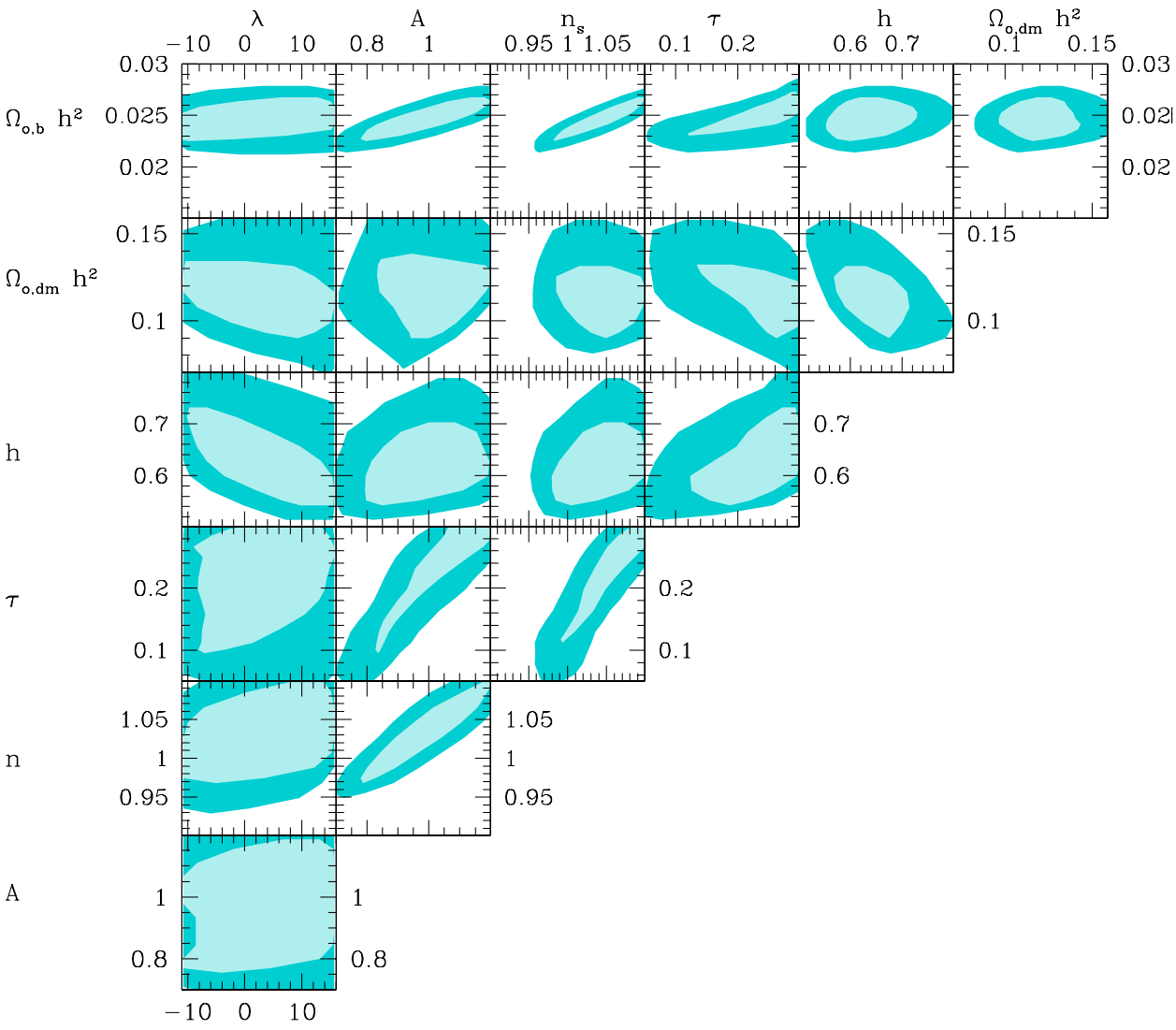


Fig. 10.— Joint 2D constraints for SUGRA models. Light (dark) shaded areas delimit the region enclosing 68.3 % (95.4 %) of the total points.

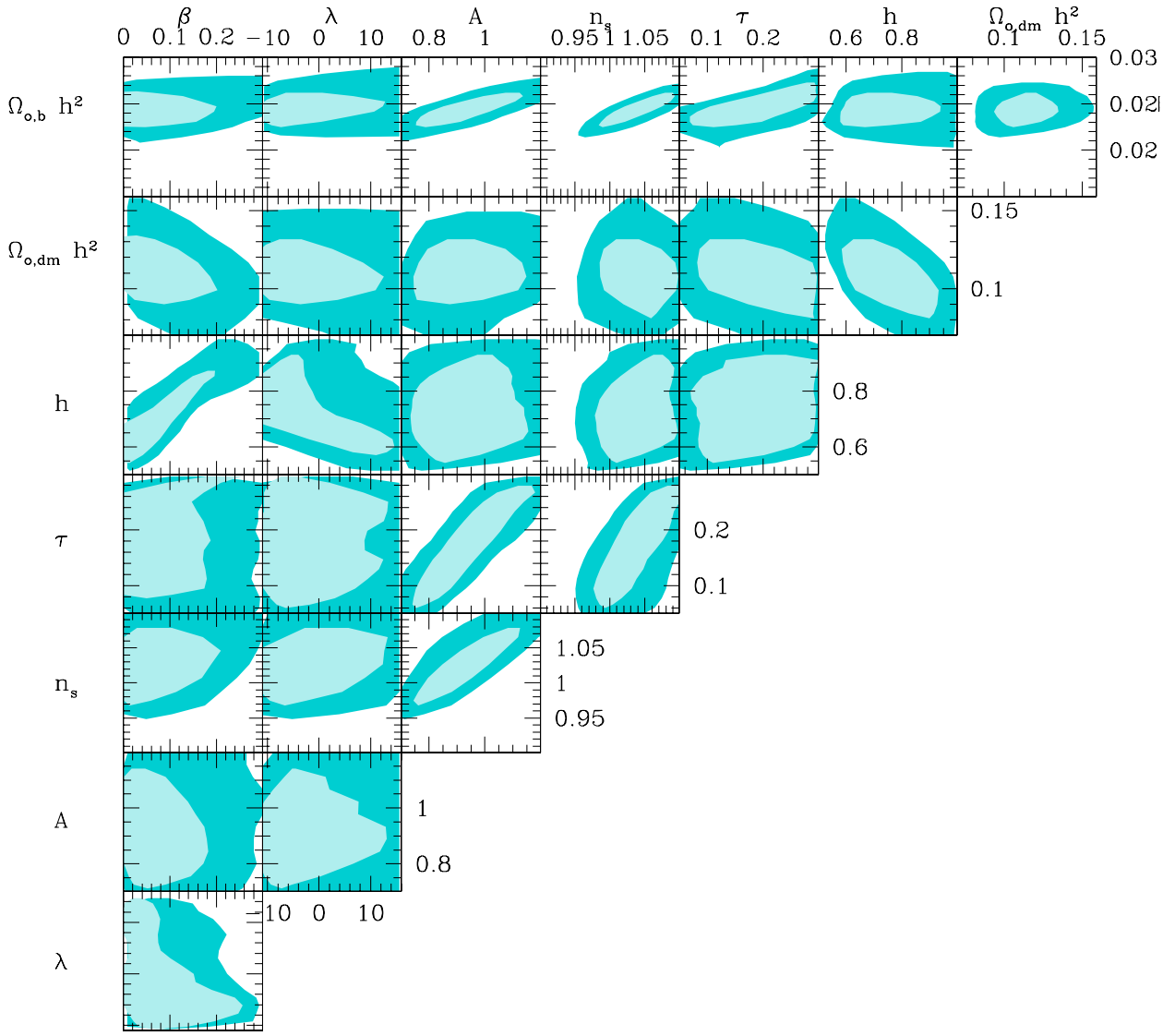


Fig. 11.— As Fig. 10 but for constant coupling models.

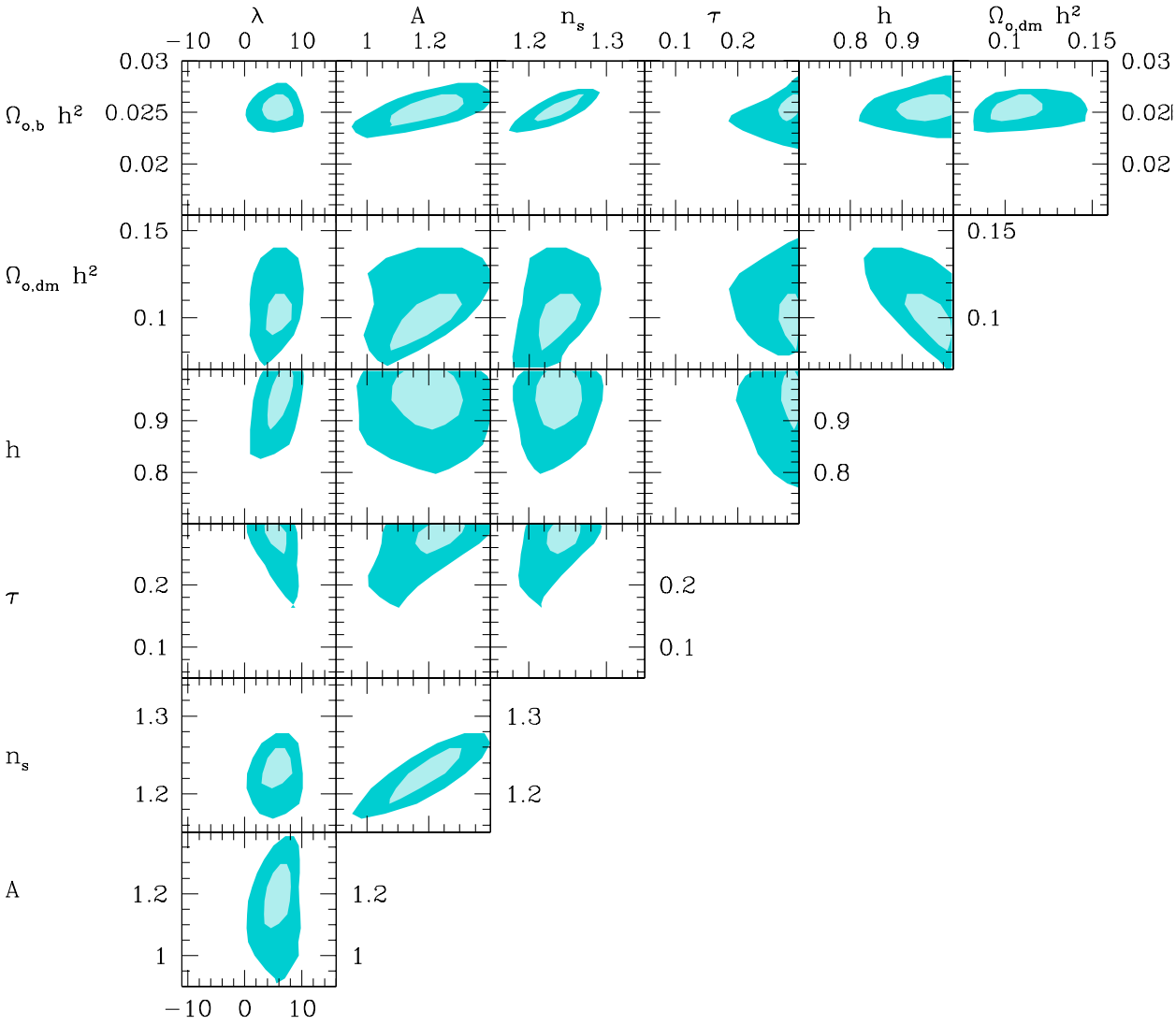


Fig. 12.— As Fig. 10 but for $\phi^{-1}$ models. Here, cosmological parameters are more stringently constrained than in other models.

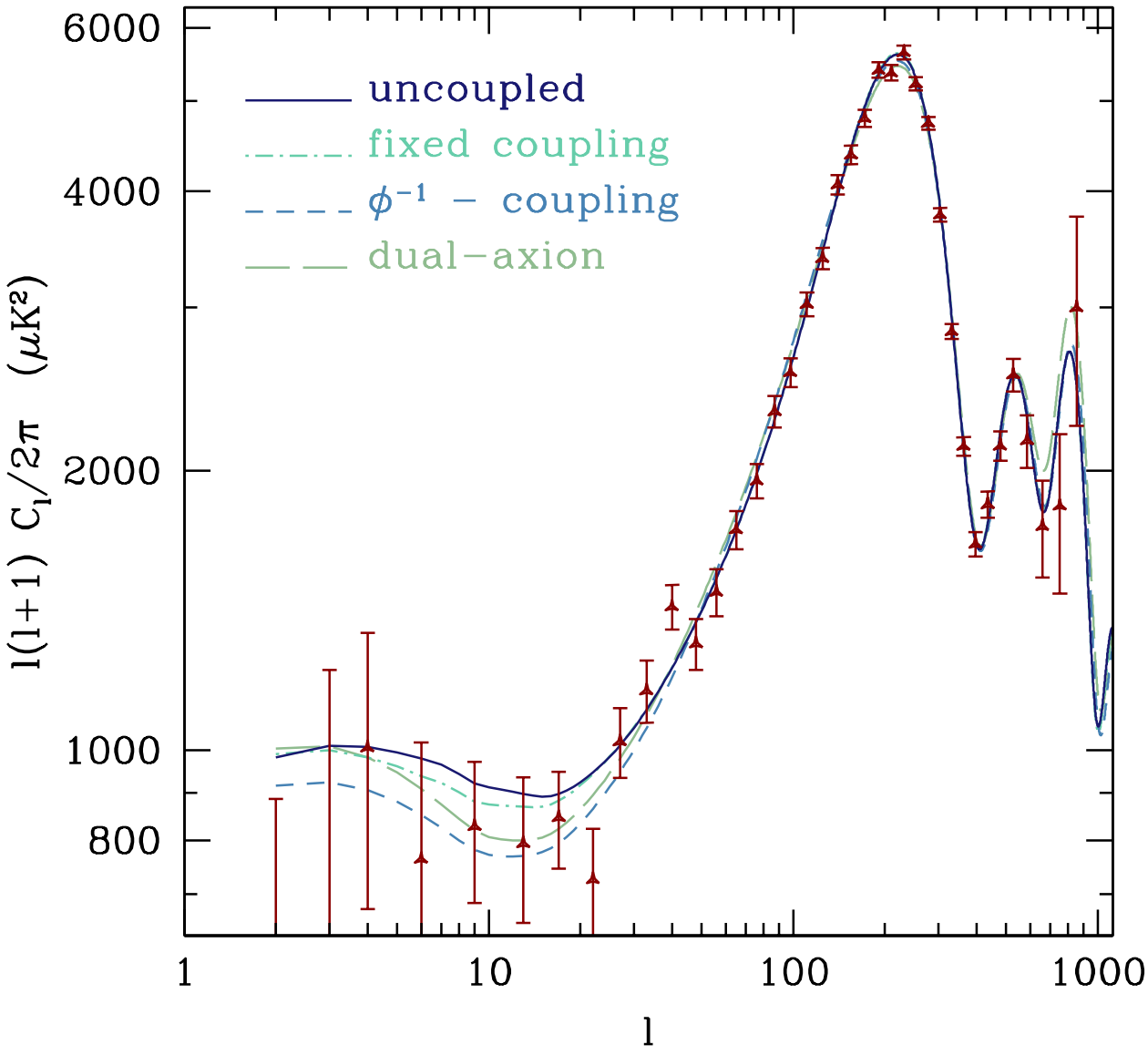


Fig. 13.— $C_l^T$ spectra for the best fit SUGRA (solid line), constant coupling (dotted line), $\phi^{-1}$–coupling (dashed) and dual–axion (dot–dashed) models. Dual–axion model results from considering only those $\phi^{-1}$ with $9.5 \leq \lambda \leq 10.5$. The binned first–year WMAP data are also plotted.

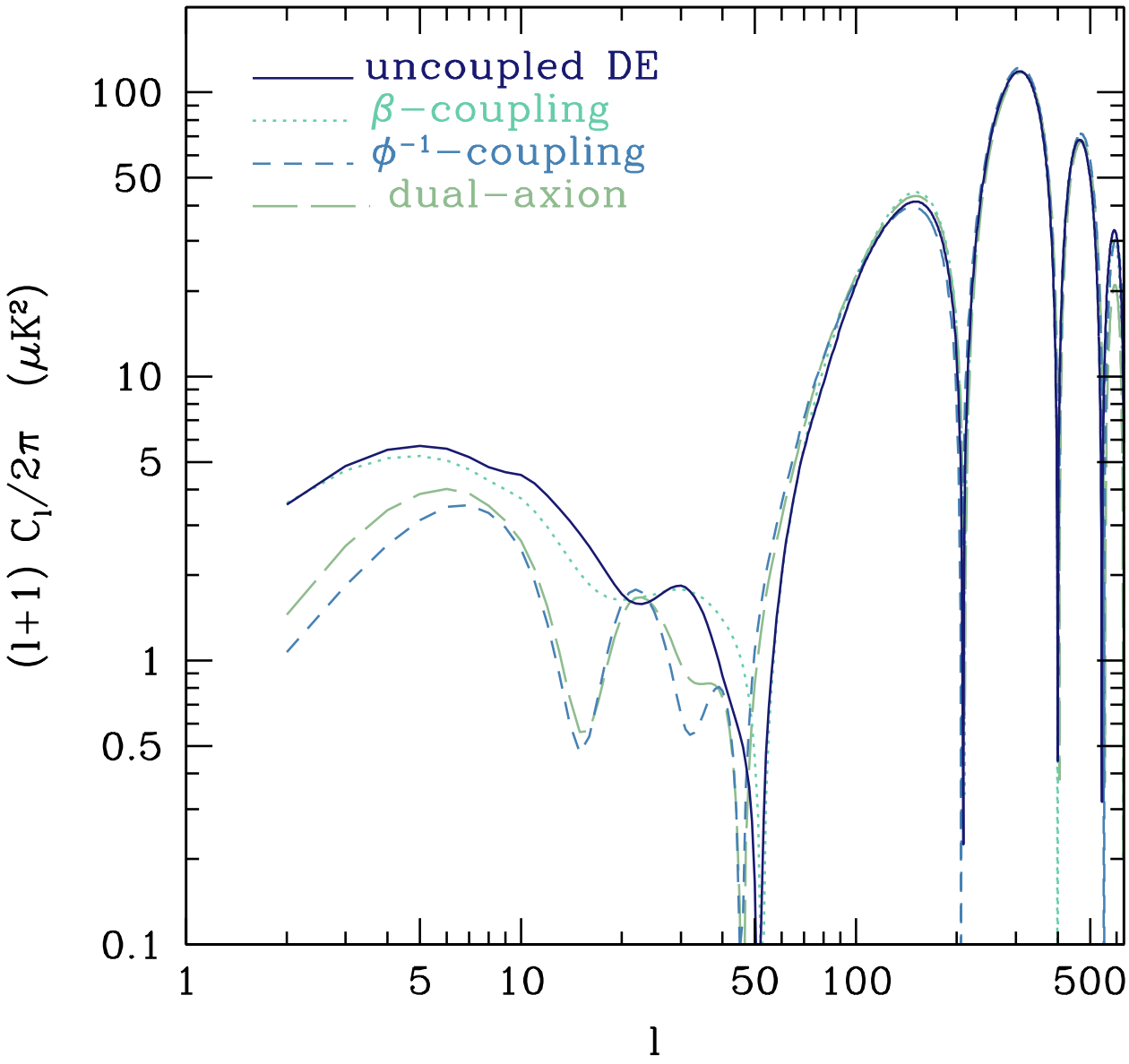


Fig. 14.— Best fit $C_l^{TE}$ spectra.

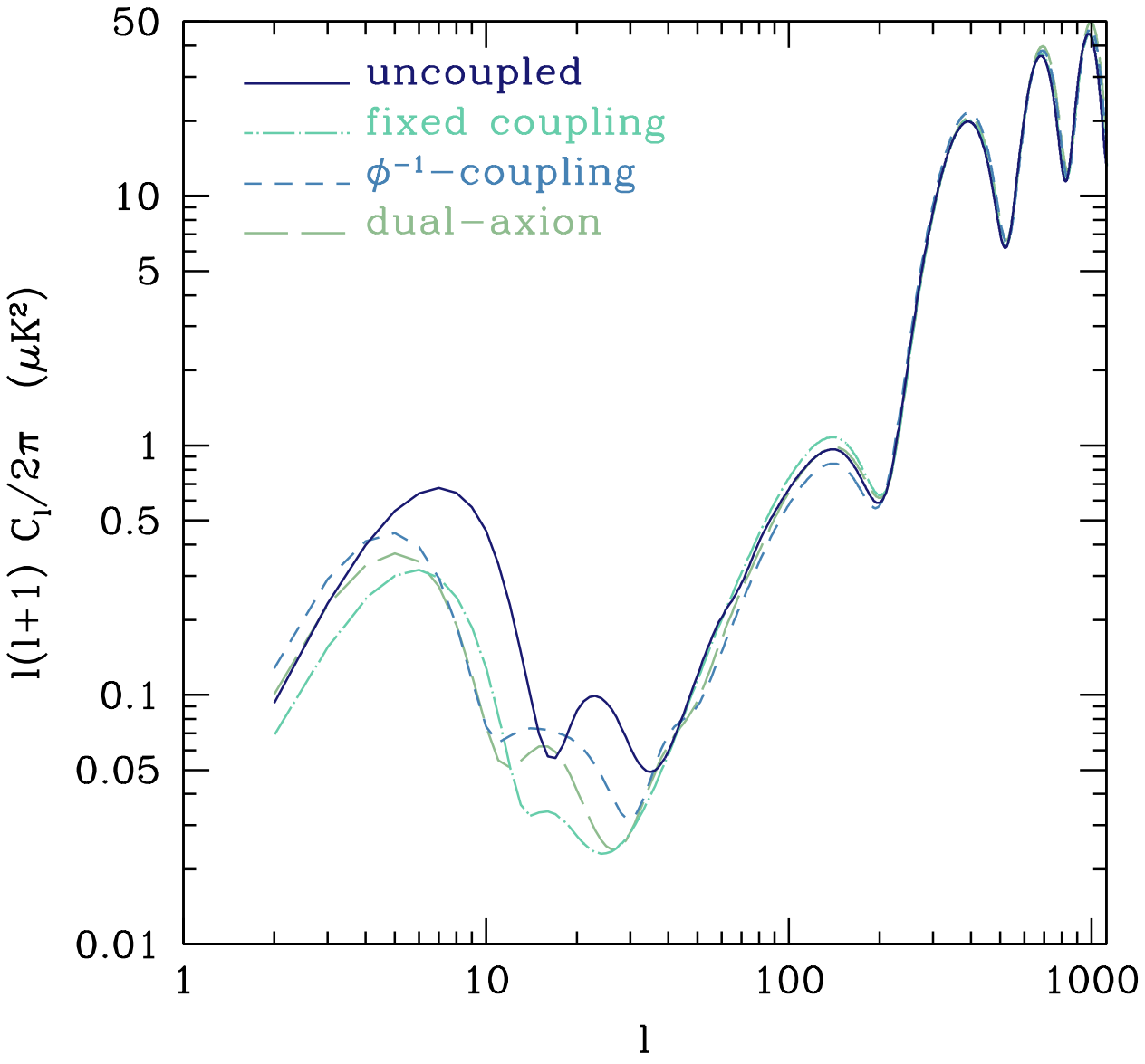


Fig. 15.— Best fit $C_l^E$ spectra.

Best fit cosmological parameters exhibit some dependence on the model. First, the opacity $\tau$ is pushed to values exceeding the $\Lambda$CDM estimates (see also Corasaniti et al. 2004). This can be understood in two complementary ways: (i) Dynamical DE models, in general, exhibit a stronger ISW effect, as the field $\phi$ itself varies during the expansion, and DE effects extend to greater $z$. This increases $C_l^T$ in the low–$l$ plateau (e.g., Weller & Lewis 2003). To compensate this effect the fit tends to shift the primeval spectral index $n_s$ to a greater value. Owing to the $\tau$–$n$ degeneracy, this is then compensated by increasing $\tau$. (ii) In dynamical DE models, the expected TE correlation, at low $l$, is smaller than in $\Lambda$CDM (Colombo et al. 2003). A given observed correlation level, therefore, requires a greater $\tau$. In any case, values of $\tau \sim 0.07$ keep consistent with data within less than 2–$\sigma$'s.

Greater $\tau$'s push upwards $\Omega_b h^2$ estimates, although best fit values are consistent with $\Lambda$CDM within 1–$\sigma$. Adding a prior on $\Omega_b h^2 = 0.0214 \pm 0.0020$ (BBNS estimates, see, e.g. Kirkman et al. 2003) lowers $h$, within 1–$\sigma$ from HST findings. We therefore also consider the effect of a prior on $h$. In Figures 7 and 8 the effects of priors are shown by the dashed red line (prior on $\Omega_b h^2$) and the dot–dashed blue line (prior on $h$).

The former prior affects mainly reionization and $n_s$; $\tau$ and $n_s$ are lowered to match WMAP's findings, the high tail of $\tau$ distribution is partly suppressed. The physical analysis of primeval objects causing reionization (e.g., Ciardi et al. 2003; Ricotti & Ostriker 2004) could however hardly account for values of $\tau \sim 0.3$ which are still allowed but certainly not *required*.

The latter prior favors greater $h$ values. In the absence of coupling, this favors low–$\lambda$ models, closer to $\Lambda$CDM. In fact, the sound horizon at decoupling is unaffected by the scale $\Lambda$, while the comoving distance to last scattering band is smaller for greater $\lambda$'s. Then, as $\lambda$ increases, lower $h$ values are favored to match the angular position of the first peak. In the presence of coupling, there is a simultaneous effect on $\beta$, as greater $\beta$'s yield a smaller sound horizon at recombination, so that the distribution on $h$ is smoother.

A previous analysis of WMAP limits on constant coupling models had been carried on by Amendola & Quercellini (2003). Their analysis concerned potentials $V$ fulfilling the relation $dV/d\phi = BV^N$, with suitable $B$ and $N$. Furthermore, they assume that $\tau \equiv 0.17$. Our analysis deals with a different potential and allows more general parameter variations. The constraints on $\beta$ we find are less severe. It must be however outlined that $\beta \gtrsim 0.1$–$0.2$ seem however forbidden by a non–linear analysis of structure formation (Macciò et al. 2004).

### 4.2. Dual–axion models

Let us consider then $\phi^{-1}$–models, which generalize dual–axion models to an arbitrary $\Lambda$ scale, used as a parameter to fit data.

Parameters are better constrained in this case, although the overall model likelihood is similar.

This is made evident by Fig. 12. In particular, at variance from the former case, the energy scale $\Lambda$ is significantly constrained and, within 2–$\sigma$, *constraints are consistent with the double–axion model.*

Several other parameters are constrained, similarly to coupled or uncoupled SUGRA models. What is peculiar of $\phi^{-1}$–models is the range of favored $h$ values: the best–fit 2–$\sigma$ interval does not extend much below 0.85 .

This problem is slightly more severe for the dual–axion model. The point is that this model naturally tends to displace the first $C_l^T$ peak to greater $l$ (smaller angular scales) as coupling does, in any case. But, in the absence of a specific coupling parameter, the very intensity of coupling, in these models, depends just on the scale $\Lambda$. Increasing $\Lambda$ requires a more effective compensation, favoring greater values of $h$.

Apart of the possibility that $h$ is currently underestimated, let us remind other substantial options which are still to be deepened: (i) The contribution of topological singularities to DM were not considered here and taking them into account could naturally increase the amount of DM, yielding smaller $\Lambda$ values for the double–axion model; fig. 6 however shows that this is hardly an efficient solution. (ii) The choice of a SUGRA potential is however arbitrary, the dual axion model does not require SUGRA. Other potentials can possibly yield the same coupling intensity in agreement with a smaller $h$.

## 5. Conclusions

The first evidences of DM date some 70 years ago, although only in the late Seventies limits on CMB anisotropies made evident that a non–baryonic component had to be dominant. DE could also be dated back to Einstein's *cosmological constant*, although only SNIa data revived it, soon followed by data on CMB and deep galaxy samples.

Axions have been a good candidate for DM since early Eighties, although various studies, as well as the occurrence of the SN 1987a, strongly constrained the PQ scale around values $10^{10} \lesssim F_{PQ} \lesssim 10^{12}$GeV. Contributions to DM from topological singularities (cosmic string and walls) narrowed the constraints to $F_{PQ}$. Full agreement on the relevance of these contributions has not yet been attained and, in this paper, they are still disregarded.

The fact that DM and DE can both arise from scalar fields, just by changing the power of the field in effective potentials, already stimulated the work of various authors. A potential like (19) was considered in the so–called *spintessence* model (Boyle et al. 2002; Gu & Hwang 2001). According to the choice of parameters, $\Phi$ was shown to behave either as DM or as DE. In the frame of a model of tachyon DE, Padmanabhan & Choudhury (2002) also built a model where DM and DE arise from a single field. The possibility that both DM and DE arise from the solution of the strong CP problem was also suggested by Barr & Seckel (2001). Their model, however, does not deal with dynamical DE and aims to explain why the vacuum energy is so finely tuned, while DM

is simultaneously provided.

Here we deal with the possibility that the $\Phi$ field, which solves the strong–$CP$ problem, simultaneously accounts for *both* DE and DM. The angle $\theta$ in eq. (1), as in the PQ model, is turned into a dynamical variable, *i.e.* the phase of a scalar field $\Phi$. While $\theta$ is gradually driven to approach zero, by our cosmic epoch, in our model $\phi$ gradually increases and approaches $m_p$, yielding DE. Residual $\theta$ oscillations, yielding axions, account for DM.

The main topic of this paper is however the fit of this and other models with WMAP data. We compared $\Lambda$CDM, SUGRA dynamical and coupled DE models, as well as a scheme we dubbed $\phi^{-1}$–model against these data. The last model encloses DM and DE and assumes that they are coupled in a non–parametric way, with $C(\phi) = \phi^{-1}$. This last model does not prescribe the origin of DE and DM, just as in standard theories of coupled DE. The fit with WMAP constrains $\Lambda$, and this constraints agree with the scale range required by the dual–axion model; thus WMAP data support the dual–axion scheme.

The fits of WMAP data to $\Lambda$CDM, uncoupled and constant–coupling SUGRA models, as well as to $\phi^{-1}$ SUGRA models, yield similar $\chi^2$'s, for all models. At variance from other model categories, however, in $\phi^{-1}$ models CMB data constrain $\Lambda$. This is due to the stronger effects of $\phi$ variations on the detailed ISW effect, as they affect both DE pressure and energy density, as well as DE–DM coupling. In principle, this strong impact of $\phi$ variation could badly disrupt the fit and make $\phi^{-1}$ models significantly farther from data. This does not occur, while the observational $\Lambda$ range agrees with the dual–axion model at a 2–$\sigma$ level.

The success would be complete if the favored range of values of the Hubble parameter ($h \sim 0.8$–1) could be slightly lowered. This range is however obtained just for a SUGRA potential. This choice is not compulsory and, moreover, contributions to axion DM due to topological singularities were also disregarded. Furthermore, primeval fluctuations were assumed to be strictly adiabatic while, in axion models, a contribution from isocurvature modes can be expected. This could legitimately affect the apparent position of the first peak in the anisotropy spectrum, so completing the success of the model, in a fully self–consistent way.

## REFERENCES

Abott L. & Sikivie P. 1983, Phys.Lett. B120, 133

Amendola L. 2000, Phys.Rev D 62, 043511

Amendola L. 2003 Phys.Rev.D (in press) and astro-ph/0311175

Amendola L. & Quercellini C. 2003, Phys. Rev. D69, 023514

arr S.M. & Seckel D. 2001, Phys. Rev. D64, 123513

Bean R. & Dorè O 2004, Phys.Rev. D69, 083503

Boyle L.A., Caldwell R.R.& Kamionkowski M. 2002, Phys. Lett. B545, 17

Brax P. & Martin J., 1999, Phys.Lett. B468, 40

Brax P. & Martin J., 2001, Phys.Rev.D 61, 103502

Brax P., Martin J. & Riazuelo A., 2000, Phys.Rev.D 62, 103505

Christensen N., Meyer R., Knox L. & Luey, B. 2001, Classical and Quantum Gravity, 18, 2677

Ciardi B., Ferrara A. & White S.D.M. 2003, MNRAS, 344, L7

Colombo L.P.L. 2004, JCAP, submitted

Colombo L.P.L., Mainini R. & Bonometto S.A. 2003, in proceedings of Marseille 2003 Meeting, 'When Cosmology and Fundamental Physics meet'

Corasaniti P.S., et al. 2004, Phys. Rev. D, in press, astro–ph/0406608

De Bernardis et al., 2000 Nature 404, 955

Dine M., Fischler W. & Srednicki M., 1981 Phys.Lett. B104, 199

Dine M., Fischler W. & Srednicki M., 1982 Phys.Lett. B120, 137

Dunkley J., et al. 2004, MNRAS, submitted, astro–ph/0405462, 2004.

Efstathiou, G. et al., 2002, MNRAS, 330, 29

Ferreira G.P. & Joyce M., 1998 Phys.Rev.D 58, 023503

Gelman A. & Rubin D.B., 1992, Statist. Sci. 7, 457

Gasperini M., Piazza F. & Veneziano G., 2002, Phys. Rev. D65, 023508

Gu Je-An & Hwang W-Y. P. 2001, Phys. Lett. B517, 1

Halverson N.W. et al. 2002, ApJ 568, 38

Hanany S. et al, 2000, ApJ 545, L5

Hinshaw G., et al. 2003, ApJ Suppl., 148, 135

Jackiw R. & Rebbi C., 1976, Phys.Rev.Lett. 37 172

Jassal H.K., Bagla J.S., & Padmanabhan T. 2004 *Preprint* astro–ph/0404378

Kim J.E. 1979, Phys.Rev.Lett. 43, 103.

Kirkman D. et al. 2003, ApJS, 149, 1

Knox L., Christensen, N. & Skordis C. 2001, ApJ 63, L95

Kogut A., et al. 2003, ApJ Suppl., 148, 161

Kosowsky A., Milosavljevic M. & Jimenez R. 2002, Phys.Rev.D 66, 63007

Lewis, A. & Bridle, S. 2002, Phys.Rev. D 66, 103511

Macciò A., Quercellini C., Mainini R., Amendola L. & Bonometto S.A. 2004, Phys. Rev. D69, 123516

Mainini, R. & Bonometto S.A., 2004, Phys. Rev. Lett. 93, 121301

Melchiorri A. 2004 Plenary Talk given at Exploring the Universe (Moriond 2004), La Thuile, March 28 - April 4, 2004 *Preprint* astro–ph/0406652

Netterfield, C. B. et al. 2002, ApJ, 571, 604

Padmanabhan T. & Choudhury T.R., 2002, Phys. Rev. D66, 081301

Peccei R.D. & Quinn H.R. 1977, Phys.Rev.Lett. 38, 1440;

Percival W.J. et al., 2002, astro-ph/0206256, MNRAS(in press)

Perlmutter S. et al., 1999, ApJ, 517, 565

Perrotta F. & Baacigalupi C., 2002, Phys. Rev. D65, 123505

Pogosian, D., Bond, J.R., & Contaldi, C. 2003, astro-ph/0301310

Preskill J., Wise M. & Wilczek F., 1982 Phys.Lett. B120, 127

Rapetti D., Allen S.W., & Weller J. 2004, MNRAS submitted, astro–ph/0409574

Ratra B. & Peebles P.J.E., 1988, Phys.Rev.D 37, 3406

Ricotti M. & Ostriker J.P. 2004, MNRAS, 350, 359

Riess, A.G. et al., 1998, AJ116, 1009

Seljak U. & Zaldarriaga M. 1996, ApJ, 469 437

Shifman M.A., Vainshtein A.I. & Zakharov V.I., 1980 Nucl.Phys. B166

Spergel D.N. et al., 2003, ApJ Suppl. 148, 175

Tegmark M., et al. 2004, Phys.Rev. D69, 10350

Tegmark M., Zaldarriaga M. & Hamilton, 2001 A.J. 63, 43007

Verde et al. 2003, ApJ Suppl., 148, 195

Weinberg S. 1978, Phys.Rev.Lett. 40, 223

Weller J. & Lewis A.M. 2003, MNRAS, 346, 987

Wilczek F. 1978, Phys.Rev.Lett. 40, 279

Wetterich C. 1988, Nucl.Phys.B 302, 668

Wetterich C. 1995, A&A 301, 32

Zhitnisky A.P., 1980 Sov.J.Nucl.Phys. 31 260